

1
2 **Dynamic and thermodynamic contribution to the October 2019 exceptional**
3 **rainfall in West Central Africa**
4

5 **Kevin Kenfack^{1*} · Francesco Marra³ · Zéphirin Yepdo Djomou^{1,2} · Lucie A. Djiotang**
6 **Tchotchou¹ · Alain T. Tamoffo⁴ · Derbetini A. Vondou¹**

7
8 ¹Laboratory for Environmental Modelling and Atmospheric Physics (LEMAP), Physics Department,
9 University of Yaoundé 1, Yaoundé, Cameroon

10 ²National Institute of Cartography, Cameroon

11 ³Department of Geosciences, University of Padova, Italy

12 ⁴Climate Service Center Germany (GERICS), Helmholtz-Zentrum Hereon, Fischertwiete 1, 20095
13 Hamburg, Germany

14
15
16 Corresponding author: **Kevin Kenfack**

17 Email: kevinkenfack46@gmail.com

18 ORCID: **0000-0003-1694-4906**

19 Kevin Kenfack's ORCID: 0000-0003-1694-4906

20 Francesco Marra's ORCID: 0000-0003-0573-9202

21 Lucie A. Djiotang Tchotchou's ORCID: 0000-0003-2860-428X

22 Alain T. Tamoffo's ORCID: 0000-0001-8482-8881

23 Derbetini A. Vondou's ORCID: 0000-0002-8681-5328

24
25 **Abstract**

26 Exceptional rainfall hit West Central Africa in October 2019. To understand the underlying
27 mechanisms, we ~~examined~~^{diagnosed} the regional moisture and Moist Static Energy (MSE) budgets
28 intending to highlight the importance of the dynamic and thermodynamic effects associated with this
29 historic event. Analysis of the moisture budget reveals that the precipitation anomalies in October
30 were mainly controlled by dynamic effects. Horizontal moisture advection induced by horizontal

31 wind anomalies controls extreme precipitation north of West Central Africa, while vertical moisture
32 advection induced by vertical velocity anomalies controls extreme precipitation south of West
33 Central Africa. Changes in the thermodynamic effect, although not the key factor responsible for the
34 events of October 2019, contribute up to 35% of the total effect on the northern part and 15% on the
35 southern part of the domain. The residual term [on the northern part \(6°N-14°N, 6°-20°E\)](#) is important
36 and provides a caveat when estimating dynamic and thermodynamic processes. Diagnosis of the
37 MSE balance averaged over the northern part of west Central Africa shows that the anomalous
38 vertical motion is dominated by the dynamic effect, i.e. the wet enthalpy advection induced by the
39 horizontal wind anomalies. This is confirmed by the high [spatial](#) correlation ($r = 0.6$) between the two
40 terms compared to the other terms. Whereas to the west of the Congo Basin, the increase in the net
41 energy balance dominated the changes in vertical motion ($r = 0.51$). The horizontal advection of the
42 MSE induced by the anomalies of the wet enthalpy and the vertical advection of the MSE induced by
43 the anomalies of the MSE seem less important ($r = 0.29$ and -0.19 to the north and -0.17 and 0.03 to
44 the south respectively). The strong anomalies in the MSE balance in the north are linked to its
45 meridional component, in particular the meridional wind anomalies in the dynamic effect and the
46 meridional anomalies in latent heat in the thermodynamic effect. Our results suggest that dynamic
47 and thermodynamic effects should be jointly considered for adequately anticipating this kind of
48 extreme event. Understanding the associated mechanisms could help us improve our [forecasts and](#)
49 [projections, projections](#) and increase the region's population resilience to these extreme weather
50 events.

51 **Keywords:** West Central Africa · Moisture budget · Moist static energy budget · Precipitation · wet
52 enthalpy

53

54

55

56

57

58 **1 Introduction**

59 Equatorial Africa recorded unprecedented amounts of rainfall in October and November 2019
60 (Wainwright et al, 2020). Such a significant amount of precipitation is not without consequences for
61 the population and the environment. In October, in most parts of East Africa in general, and in Kenya

62 in particular, extreme rainfall led to flooding and landslides, provoking major destruction, with more
63 than 100 deaths and around 18,000 people displaced internally and to neighbouring countries
64 (<http://floodlist.com/africa/kenya-floods-november-2019>). In Central Africa, the Democratic
65 Republic of Congo has been devastated by major flooding and forestry disruption along the Congo
66 River, forcing many people to move (Gou et al. 2022). In the Central African Republic, extreme and
67 persistent rainfall caused significant flooding and landslides, including the Oubangui River
68 overflowing nearly 60 km of its coastline (Igri et al. 2023). In addition, the night of 27 to 28 October
69 2019 was disastrous in the West Cameroon region, mainly in the locality of Bafoussam where
70 extreme rainfall for about 36 hours caused a landslide, resulting in significant material damage with
71 45 dead and others missing (Aretouyap et al. 2021; Mfondoum et al. 2021; Wantim et al. 2023). The
72 episode was associated with a thermal depression over the Sahara and with anomalously high Sea
73 Surface Temperatures (SST). The occurrence of these conditions may change in response to
74 anthropogenic global warming, raising the question of whether devastating events such as the one of
75 October 2019 could occur more frequently in the future (Nicholson et al. 2022). In particular, given
76 that climate models predict an increasing trend in extreme rainfall in the region (Fotso-Nguemo et al.
77 2018, 2019; Sonkoué et al. 2018; Tamoffo et al. 2019, 2023) and that extreme precipitation in the
78 region is associated with vegetation dynamics (Zhou et al. 2014; Mariotti et al. 2014; Marra et al.
79 2022; Garcin et al. 2018), it is crucial to understand the thermodynamic and dynamic mechanisms
80 underlying these exceptional events of October 2019.

81 Recent studies have attempted to investigate the causes of extreme rainfall during the exceptional
82 period of October 2019 in Equatorial Africa. Nicholson et al. (2022) showed that the heavy rainfall
83 on the Guinean coast was reinforced by positive sea surface temperature anomalies along the Atlantic
84 coast. This process leads to a significant advection of the moisture flux from the Atlantic, combined
85 with the convergence of the moisture, which contributed to the increase in rainfall in the region
86 (Pokam et al. 2011, Kuete et al. 2019). Wainwright et al. (2020) pointed out that the increase in
87 rainfall over East Africa was a consequence of the positive phase of the Indian Ocean Dipole. Indeed,
88 Black et al. (2005) reported that during periods of the year when the dipole mode index (DMI) IOD
89 events are greater than 0.5°C over a period of 3 consecutive months and when the zonal SST gradient
90 is reversed over several months, the resulting increase in rainfall over East Africa is important. In
91 addition, the positive IOD event of 2019 lasted from late summer through to December, influencing
92 rainfall over East Africa.

93 Rainfall variability in Central Africa is highly dependent on the convergence of atmospheric
94 moisture (Pokam et al. 2012; Washington et al., 2013; Dyer et al., 2017; Hua et al., 2019; Taguela et
95 al. 2022; [Tamoffo et al. 2023b,2024](#)). Under the effect of global warming, the increase in extreme

96 precipitation is a consequence of the increase in available atmospheric humidity (Nicholson et al
97 2022). Although previous studies have focused on analyzing meteorological factors, there is still a
98 general lack of knowledge about quantifying the dynamic and thermodynamic effects associated with
99 these extremes of precipitation. In recent years, the decomposition of the water balance behind
100 precipitation anomalies is often used to isolate the dynamic and thermodynamic contributions to
101 extreme events (Li et al., 2017; Oueslati et al., 2019; Wen et al., 2022; Kenfack et al., 2023,2024).
102 Water balance analysis has proved to be a useful tool for understanding anomaly fields in mean
103 precipitation under the influence of global warming (Seager et al. 2014). Moist static energy (MSE),
104 in particular, is a useful parameter for investigating the contribution of atmospheric moisture and
105 ~~analysing~~ analyzing vertical velocity (Wang and Li, 2020a, 2020b; Bell et a. 2015; Neelin, 2021;
106 Nana et al. 2023; Andrews et al. 2023; Longandjo and Raoul, 2024; Kenfack et al. 2024). Recently,
107 Kenfack et al. (2024) showed that, in the Congo Basin, the structure of the horizontal moisture
108 advection anomalies is similar to that of the MSE advection anomalies during rainy seasons March-
109 April-May (MAM) and September-October-November (SON). In addition, the atmospheric heating
110 source has been identified as an indicator of precipitation (He et al. 2021). The increase in diabatic
111 heating on the coast can contribute to the acceleration of near-surface winds (Pokam et al. 2014). An
112 increase in this quantity implies an increase in latent warming, associated with a strong ocean-
113 continent horizontal moisture gradient, which can lead to a strengthening of the boundary layer MSE,
114 with a positive feedback process leading to extreme precipitation. Further, it has been demonstrated
115 that a simultaneous reduction in the heating source and rainfall has been observed in reanalyses over
116 recent decades in the Congo Basin (Kenfack et al. 2024). Given the highlighted importance of
117 moisture, MSE and heating sources on rainfall variability, we adopt in this study an approach based
118 on diabatic heating, water balance and MSE to diagnose dynamic and thermodynamic processes
119 associated with the October 2019 rainfall extremes over West Equatorial Africa.

120 The remainder of the paper is structured as follows. A description of the observation and
121 reanalysis data, and analysis methods is presented in Section 2. Section 3 describes the diabatic
122 heating source and the performance of the reanalysis in capturing the October 2019 precipitation
123 extremes. In Section 4, we investigate the dynamic and thermodynamic effects associated with the
124 moisture balance. The analysis of the dynamic and thermodynamic effects associated with the MSE
125 budget during the October 2019 rainfall anomaly period over West Central Africa is presented in
126 Section 5. Section 6 is conclusions and discussions.

127

128 **2 Data and methods**

129 2.1. Data

130 In this study, datasets from the fifth version of the European Centre for Medium-Range Weather
131 Forecasts reanalysis, known as ERA5 (Hersbach et al., 2020), are used for the analyses. Johannsen
132 et al. (2019) established that over equatorial Africa, ERA5 significantly improves over ERA-
133 Interim (which represents the previous dataset), particularly in the description of the hydrological
134 cycle. In addition, Cook and Vizy (2021) have shown that ERA5 represents well the spatial
135 distribution of precipitation and atmospheric dynamic fields compared with previous generations,
136 particularly over the Congo Basin. With a spatial resolution of $0.25^\circ \times 0.25^\circ$, ERA5 is a global
137 reanalysis dataset available from 1979 to the present, covering 137 pressure levels from the surface
138 to 0.01 hPa. Monthly variables including horizontal and vertical wind components, geopotential,
139 evaporation, humidity, heat flux and temperature are used in this study. For all variables, anomalies
140 are obtained by removing the 30-year mean of the period 1988 to 2017. In order to reinforce the
141 robustness of the results, several variables, such as winds (horizontal and vertical), specific
142 humidity, precipitation and evaporation, obtained from the Modern-Era Retrospective Analysis for
143 Research and Applications, version 2 (MERRA2), which provides data from 1980 to the present
144 day (Gelaro et al., 2017), were used in this study. To assess ERA5's ability to detect October 2019
145 precipitation extremes, we used three observational datasets, including rain gauge products and
146 gauge-adjusted satellite products: the Climate Hazards Group InfraRed Precipitation with Stations
147 (CHIRPS) gridded dataset, available at a resolution of $0.05^\circ \times 0.05^\circ$ (Funk et al., 2015); the Global
148 Precipitation Climatology Project (GPCP-v2.2) with a grid spacing of $2.5^\circ \times 2.5^\circ$ (Huffman et al.,
149 2009); the Climatic Research Unit (CRU-TS4.03) gridded data at a resolution of $0.5^\circ \times 0.5^\circ$ (Harris
150 et al., 2020).

151

152 2.2 Methods

153 2.2.1 Diabatic heating

154 Apparent diabatic heating as proposed by Yanai and Tomita (1998) and Pokam et al. (2014) is
155 defined as follows:

$$156 \quad Q = \chi \left(\frac{\partial \theta}{\partial t} + u \frac{\partial \theta}{\partial x} + v \frac{\partial \theta}{\partial y} + \omega \frac{\partial \theta}{\partial p} \right) \quad (1)$$

$$157 \quad \chi = c_p \left(\frac{T}{\theta} \right) \quad (2)$$

158 In equations 1 and 2, C_p ($1,005 \text{ J Kg}^{-1} \text{ K}^{-1}$) denotes the specific heat at constant pressure, θ is the
159 potential temperature, ω is the vertical velocity (hPa s^{-1}), and $V=(u, v)$ is the vector of horizontal
160 velocities. T (K) and p (hPa) represent the air temperature and the barometric pressure, respectively.

161 To quantify the monthly mean heating rate τ ($K day^{-1}$) related to apparent heating, we use the
 162 relation:

$$163 \quad \tau = \frac{Q}{c_p} \quad (3)$$

164 where Q is the combination of heat from radiation, latent heat from condensation and the
 165 convergence of vertical vortical transport of sensible heat.

166

167 2.2.2 Diagnosis of the moisture budget

168 The moisture budget used to quantify the contributions of evaporation and the horizontal and
 169 vertical components associated with the circulation of moist air in the atmosphere (Seager et al.,
 170 2010; Oueslati et al., 2019; Jiang et al., 2020; Moon and Ha, 2020; Wen et al., 2022; Zhao et al.,
 171 2022; Sheng et al., 2023; Kenfack et al., 2024) is defined as follows:

$$172 \quad \langle \partial_t q \rangle + \langle V \cdot \nabla_h q \rangle + \langle \omega \cdot \partial_p q \rangle = E - P \quad (4)$$

173 In Eq. 4, q represents the specific humidity, $V=(u,v)$ denotes the horizontal wind and ω the vertical
 174 pressure velocity. E denotes surface evaporation and P precipitation. Angle brackets " $\langle \rangle$ "
 175 signify the mass integral from the surface ($p_s = 1000$ hPa) to a pressure $p_t = 300$ hPa ,
 176 which represents the top of the atmosphere layer considered. The first term on the left of equation 4
 177 can be neglected given its small variation over time on a monthly scale and could contribute to the
 178 residuals (Wen et al. 2022; Sheng et al. 2023). To estimate the horizontal and vertical moisture
 179 advection components, we decompose equation 4 into its different linear and residual terms as
 180 follows:

$$181 \quad P' = E' - \langle \nabla \cdot \nabla q' \rangle - \langle V' \cdot \nabla \bar{q} \rangle - \langle \bar{\omega} \partial_p q' \rangle - \langle \omega' \partial_p \bar{q} \rangle + Res \quad (5)$$

182 In Eq. 5, the overbar indicates the monthly mean climatology from 1988 to 2017 and primes
 183 indicate deviations from this climatology; The residual term "Res" contains the non-linear and
 184 transient processes associated with the joint variations in water vapor content and circulation. The
 185 terms $\langle -V' \cdot \nabla \bar{q} \rangle$ and $\langle -\omega' \partial_p \bar{q} \rangle$ represent the dynamic contributions (or effect) and refer to
 186 the moisture advection induced by the horizontal wind and by the vertical pressure velocity,
 187 respectively. The terms $\langle -\nabla \cdot \nabla q' \rangle$ and $\langle -\bar{\omega} \partial_p q' \rangle$ represent the thermodynamic contributions
 188 (or effect), and refer to the contribution of water vapor.

189

190 2.2.3 Diagnosis of the MSE budget

191 The MSE equation is defined as follows:

$$\langle \partial_t (c_v T + L_v q) \rangle + \langle V \cdot \nabla M \rangle + \langle \omega \partial_p m \rangle = F_{net}$$

$$\langle \partial_t (c_v T + L_v T) \rangle + \langle V \cdot \nabla M \rangle + \langle \omega \partial_p m \rangle = F_{net} \quad (6)$$

where the moist enthalpy is

$$M = c_p T + L_v q \quad (7)$$

and the MSE is

$$m = c_p T + L_v q + \Psi \quad (8)$$

In equations 7 and 8, c_p (c_v) represents the specific heat at constant pressure (the specific heat at constant volume); T is the air temperature and Ψ the geopotential. F_{net} is the net energy entering the atmospheric column at the surface and top of the atmosphere (latent heat, sum of sensible heat, and shortwave and longwave radiative fluxes). Similar to the moisture flux equation, the first term on the left of equation 6 can be neglected given its small variation over time on a monthly scale and contributes to the residuals. In addition, it should be noted that variations in geopotential height along pressure levels are neglected in this formulation of the MSE budget. The remaining terms in equation 6 can be decomposed into horizontal and vertical advection components, as described by:

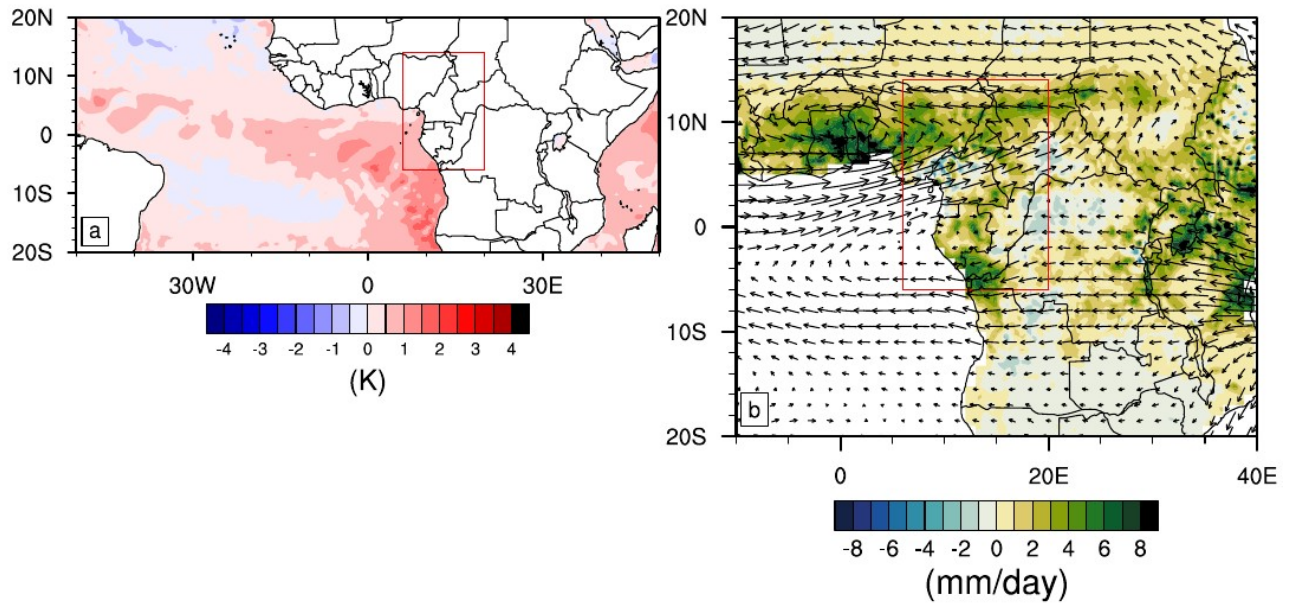
$$\langle \omega' \partial_p \bar{m} \rangle = -\langle V \cdot \nabla M' \rangle - \langle V' \cdot \nabla M \rangle - \langle \omega \partial_p m' \rangle + F'_{net} + Res \quad (9)$$

Anomalous vertical motion is analysed using this equation with a given profile of \bar{m} . Similar to the convention adopted for decomposing the moisture flux, the term $-\langle V' \cdot \nabla M \rangle$ relates to the anomalous MSE associated with the atmospheric circulation and contains the dynamic contribution (or effect), while the two terms $-\langle V \cdot \nabla M' \rangle$ and $-\langle \omega \partial_p m' \rangle$ refer to the thermodynamic contribution (or effect), which is crucial for diagnosing the thermal state of the atmosphere associated with the increase in the vertical rise of the air.

213

214 | 3 Diabatic heating and extreme rainfall

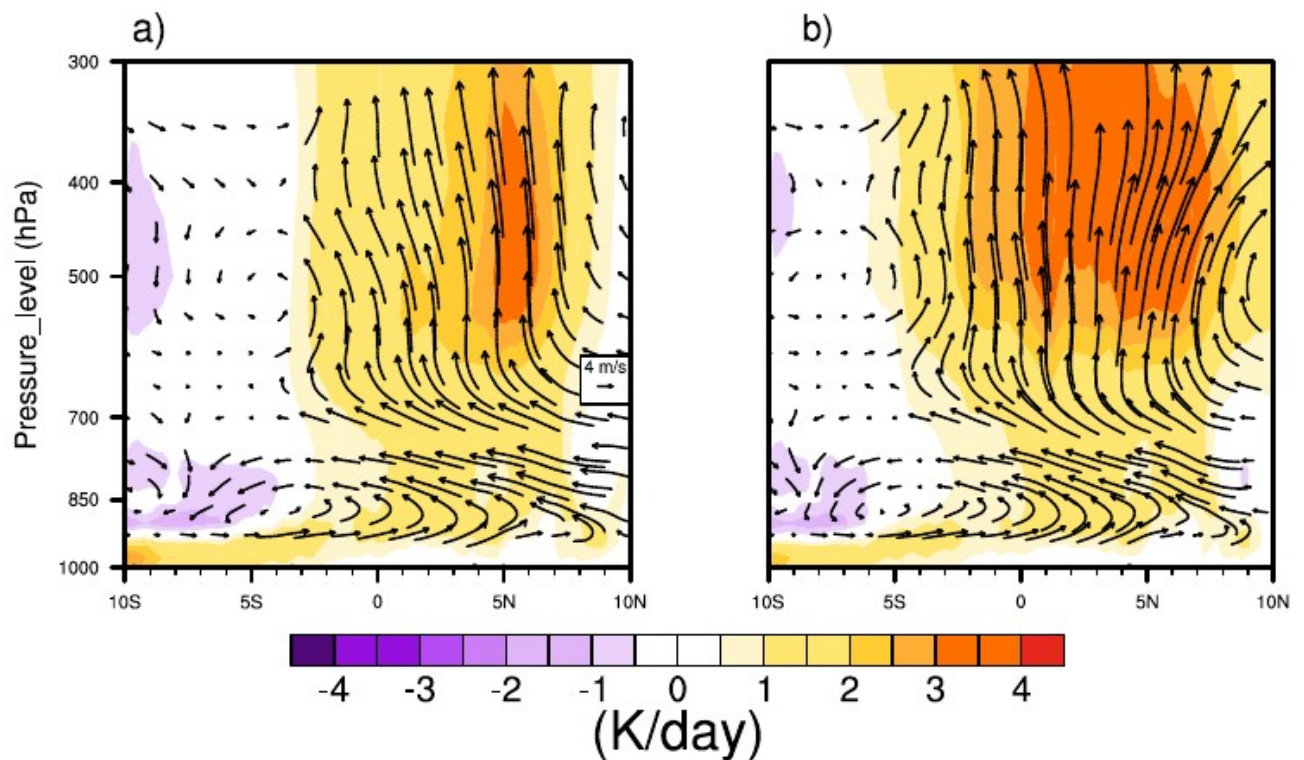
215 | The increase in SSTs in the eastern Atlantic (Fig. 1a) [has been](#) identified as one of the causes of
 216 | the positive precipitation anomalies over western central Africa in October 2019. The warming
 217 | contrast between the ocean and the continent favoured the strengthening of the moisture advection
 218 | associated with the precipitation anomalies over West Central Africa (Fig. 1b). This is in agreement
 219 | with Nicholson et al. (2022).



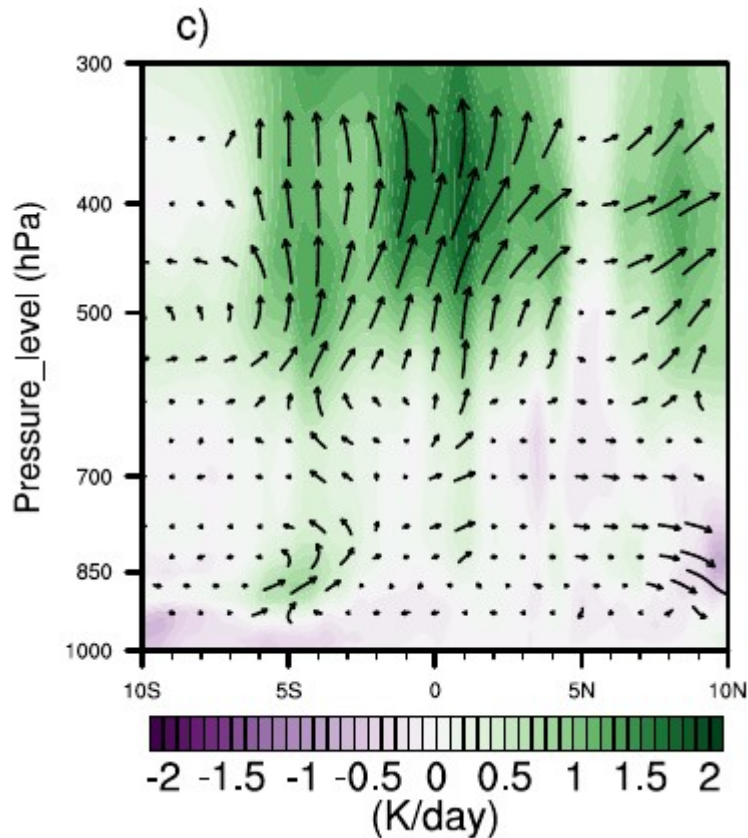
220

221 **Fig 1.** SST a) and rainfall b) anomalies during October 2019. The vectors represent anomalies of
 222 vertically integrated atmospheric moisture flux. The red box indicates the Central West Africa area.

223 Figure 2 represents the mean vertical profile (pressure-latitude) of diabatic heating averaged
 224 between 6° and 20°E during SON for the 1988-2017 climatology (Fig. 2a) and the corresponding
 225 profile for 2019 (Fig. 2b). During SON, the main source of heat is located between 3°S and 9°N for
 226 climatology, and between 5°S and 13°N for 2019.



227



228

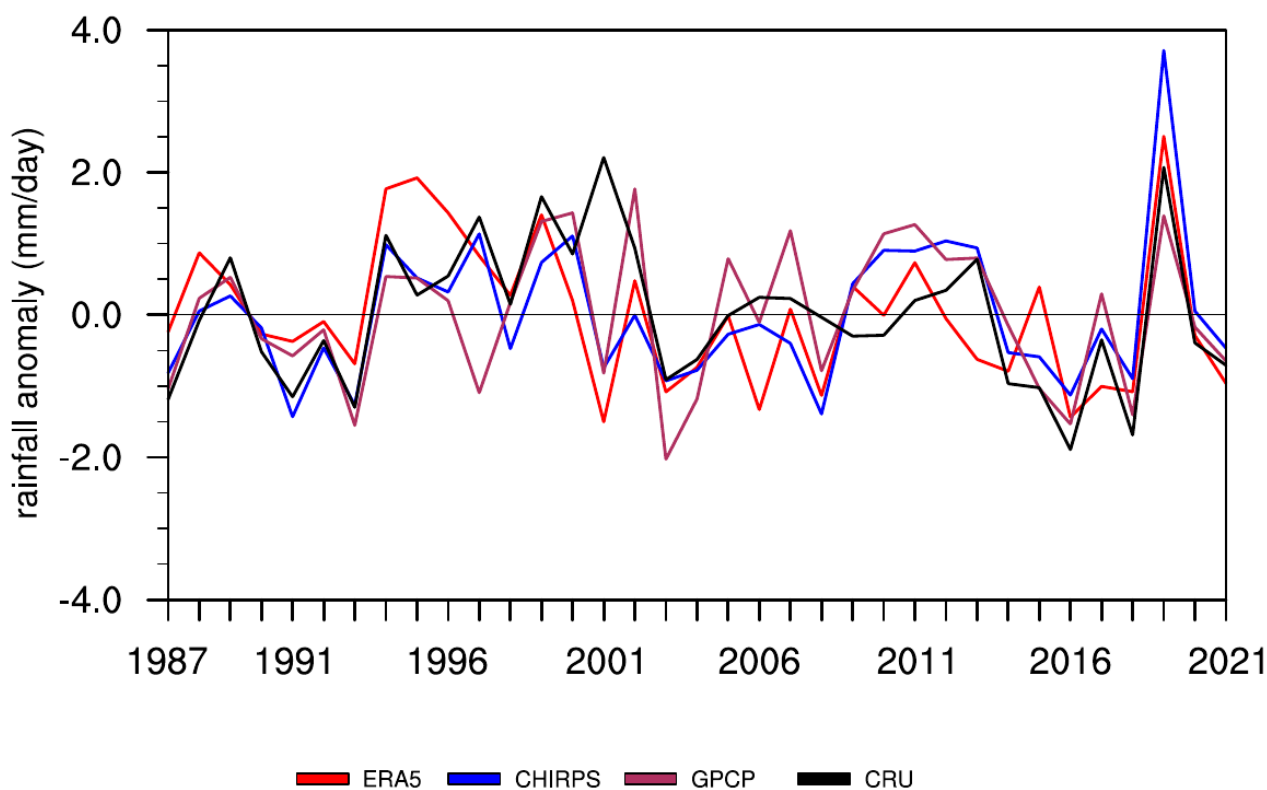
229 **Fig 2.** Diabatic heating and divergent meridional circulation (vectors; $m s^{-1}$) during the SON
 230 season for a) 1988-2017 avg, b) 2019 avg and c) the anomaly, all averaged between the 6° and
 231 20°E. As the vertical velocity is much weaker than the meridional wind, its values have been
 232 enhanced by a factor of 600 for the clarity of the graph.

233

234 However, 2019 presents a more extensive and pronounced source of heat compared with the
 235 climatology 1988-2017. A $3-4 K day^{-1}$ heating, more intense in 2019, occurred from 600 hPa. A
 236 cooling of $1-2 K day^{-1}$ took place around 850 hPa in the south and from 550 hPa in the north. The
 237 profound heating observed from 600 hPa originates at the surface on the southern portion of the
 238 domain (10°S). It is reinforced by the contrast between the large positive values and the negative
 239 values on either side of the equator between 500 and 400 hPa. The vertical structure of the
 240 divergent circulation is also illustrated in Figure 2. The divergent circulation appears more
 241 pronounced from 550 hPa in 2019 (Fig. 2b) compared with the climatology of 1988-2017 (Fig. 2a).
 242 This is consistent with the warming contrast observed. This uplift was reinforced by the warming of
 243 the equatorial Atlantic associated with an abnormally strong thermal low over the Sahara, which led
 244 to an acceleration of the dominant meridional flow in the divergent circulation (Fig. 2c). This is in

245 agreement with Nicholson et al. (2022), who highlighted that the West African monsoon was late to
246 withdraw in 2019.

247 Although the SON season has shown significant diabatic heating compared to climatology,
248 October 2019 in particular over West Central Africa recorded extremes of rainfall (Nicholson et al.
249 2022). In this study, we use the ERA5 reanalysis precipitation fields for water balance analysis.
250 This ensures that all the examined physical quantities are consistent across the study. Before doing
251 so, we assessed the performance of ERA5 in detecting the extreme precipitation events in October
252 2019. Figure 3 illustrates the interannual variability of October rainfall anomalies over West Central
253 Africa for the period 1987-2021.

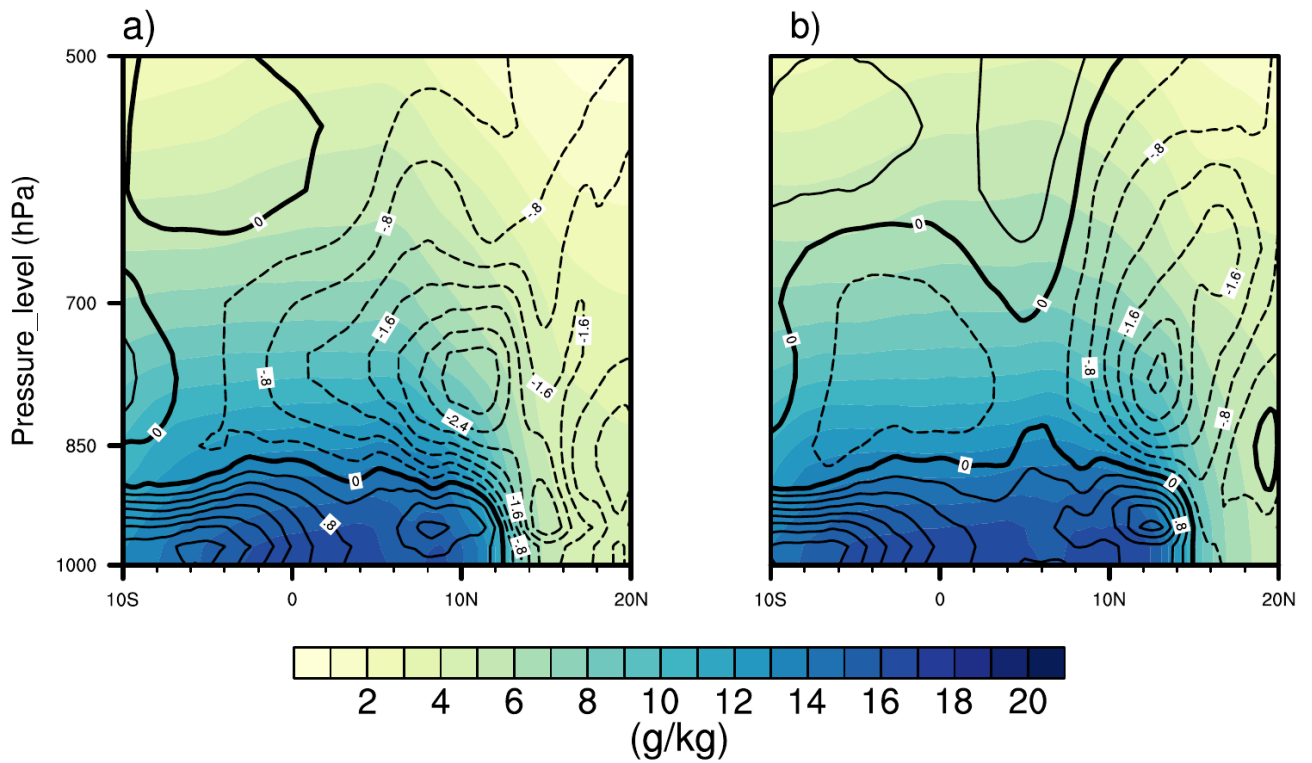


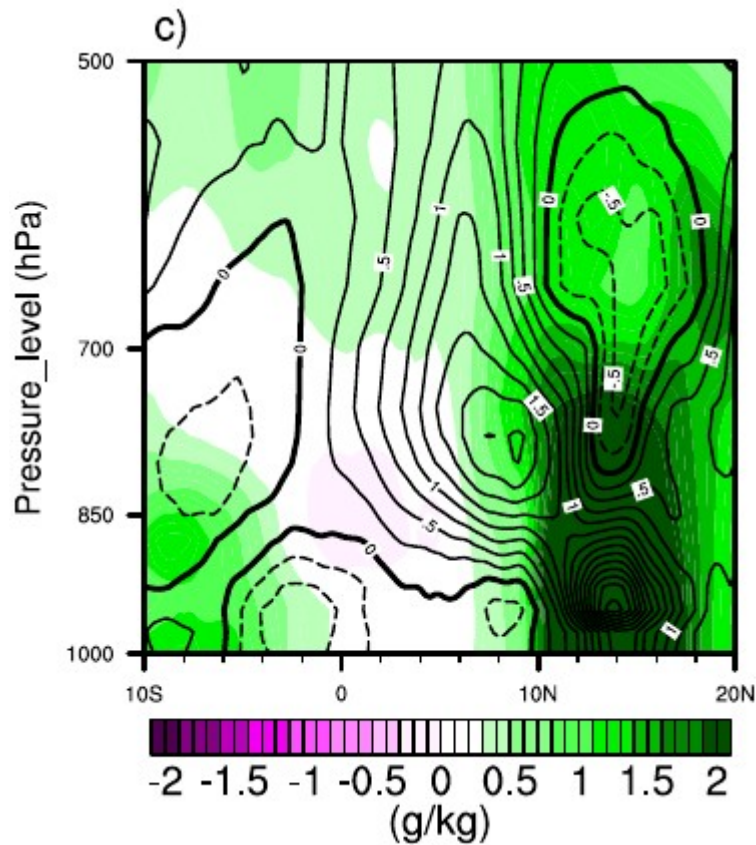
254
255 **Fig 3.** Temporal evolution of October rainfall anomaly over West Central Africa (6°S-14°N, 6°-
256 20°E), from reanalysis data ERA5 (red) and from observational data CHIRPS (blue), GPCP
257 (maroon) and CRU (black), covering the period 1987–2021.

258
259 The ERA5 reanalysis (red) and the CHIRPS (blue), GPCP (maroon) and CRU (black) observations
260 are consistent in highlighting the high precipitation peak of 2019. CHIRPS shows the highest values
261 of positive anomalies of up to 3.5 mm day⁻¹, while ERA5 shows values of up to 2.5 mm day⁻¹.
262 Despite some differences between ERA5 and the observations in representing trends on an

263 interannual scale (Kenfack et al. 2024), the unprecedented event of October 2019 was well detected.
264 In addition, the exceptional event is also detected by the MERRA2 reanalysis (Figure S1)

265 The increase in SSTs in the tropical Atlantic reached a record level in October 2019
266 (Nicholson et al. 2022). This may have resulted in an increased specific humidity over land. Figure
267 4 depicts the vertical profile (pressure level-latitude) of specific humidity (colors) and meridional
268 wind (contours) averaged between 6° and 20°E for the 1988-2017 climatology (Fig. 4a), the
269 October 2019 average (Fig. 4b), and the October 2019 anomaly (Fig. 4c).





271

272 **Fig. 4.** Specific humidity and meridional wind (contours: m/s) in October for a) 1988-2017 avg, b)
 273 2019 avg and c) the anomaly, averaged between 6°-20°E.

274

275 The 1988-2017 climatology is characterized by intense surface specific humidity extending as far as
 276 12°N, whereas the October 2019 average appears to extend further to 15°N. In addition, the
 277 southerly wind in 2019 was more pronounced up to 15°N compared to the climatology. Analysis of
 278 the anomalies confirms that the humidity extended further north in West Central Africa in October
 279 2019, compared with the climatology. The intensification of the southerly wind up to 15°N
 280 indicates that this moisture probably comes from the equatorial Atlantic. This is in agreement with
 281 Kamae et. al (2017), who highlighted that extreme precipitation can be a consequence of changes in
 282 humidity. Indeed, the increase in humidity associated with a substantial heating source contributes
 283 to an increase in precipitation. ~~In addition, In the case of the monthly anomalies, the changes in the~~
 284 ~~winds are thought to be a response to the increased moisture advection from the oceans as a result~~
 285 ~~of global warming.~~

286

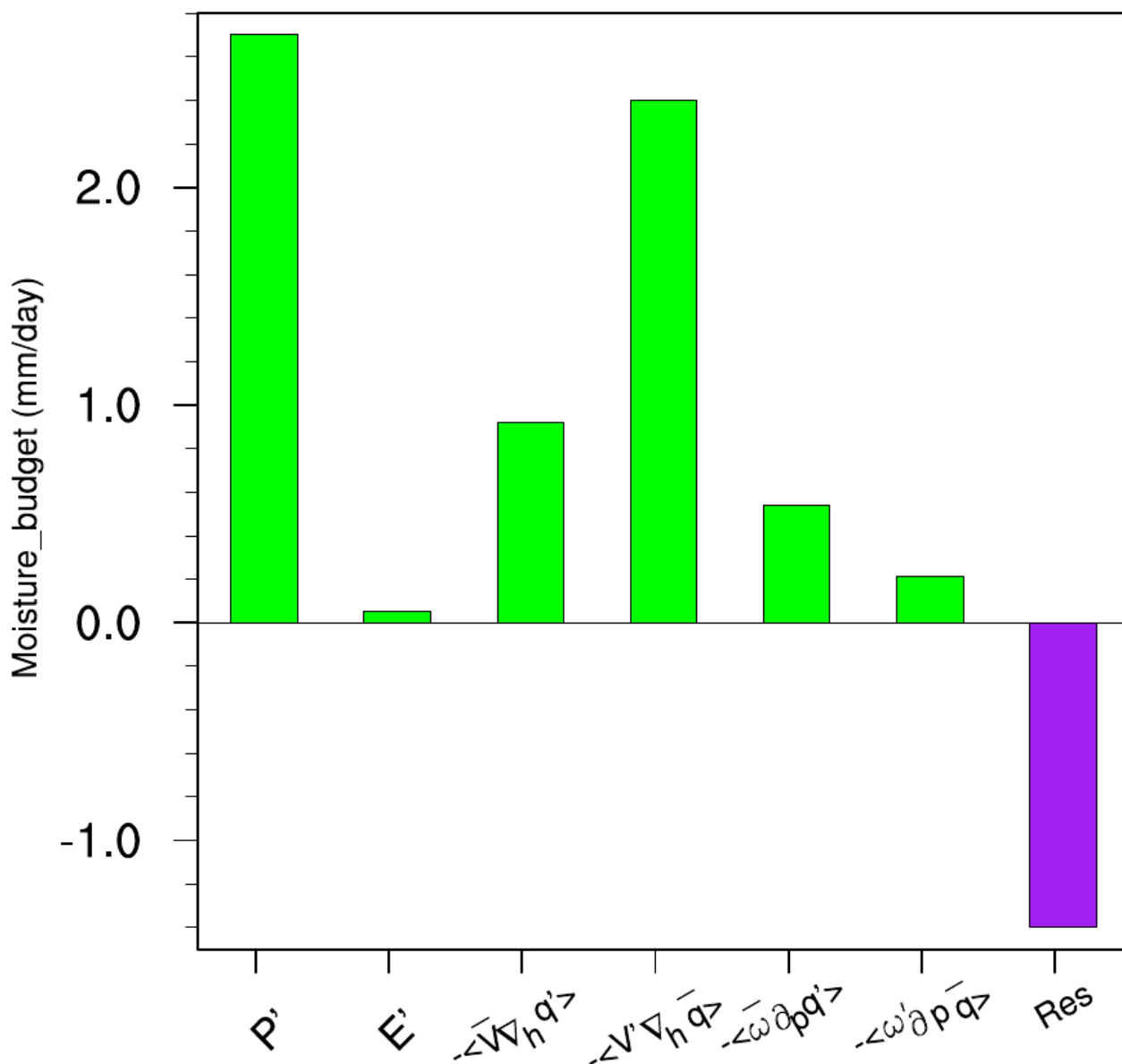
287

289 Rainfall variability in equatorial Central Africa is strongly dependent on the moisture inputs
 290 associated with atmospheric circulation (Jackson et al., 2009; Cook and Vizy, 2016, 2022; Dyer et
 291 al., 2017; Longandjo and Raoul, 2024). In the Congo Basin, atmospheric heating sources combined
 292 with the vertical advection of moisture induced by anomalous vertical motion are responsible for
 293 most of the interannual variability of precipitation (Kenfack et al., 2024). In this section, we
 294 decompose the moisture budget in equation 5 to examine the processes that led to the October 2019
 295 extreme rainfall over West Central Africa. To do this, we analyse local variations in rainfall
 296 associated with atmospheric moisture introduced into the air column by atmospheric circulation.

297 The monthly anomalies of the different components of the water balance averaged over the
 298 northern part of west-central Africa (6°N-14°N, 6°-20°E) for the month of October 2019 (Fig. 5a5)
 299 indicate that the increase in dynamic processes dominated the increase in precipitation. Horizontal
 300 advection of moisture induced by the horizontal wind anomaly $\langle -\mathbf{v}' \cdot \nabla \bar{q} \rangle$ was the most
 301 pronounced component (up to 2.5 mm/day). Although thermodynamic processes $\langle -\nabla \cdot \nabla q' \rangle$ and
 302 $\langle -\omega \partial_p q' \rangle$ are weaker than dynamic processes, they also contributed to the extreme rainfall
 303 amounts. Evaporation E , for its part, contributed very little (0.1 mm/day). This is consistent with
 304 Cook et al. (2019) who found that rainfall anomalies in equatorial Central Africa do not depend
 305 directly on surface heating. It should also be noted that the residual term for a value of -1.2 mm/day
 306 is considerable. Indeed, the northward shift and strengthening of the northern component of the
 307 East African Jet (AEJ-N) in October are verified (Nicholson et al. 2022). This is illustrated by the
 308 anomalous 700 hPa zonal wind in October 2019. In addition, the anomalous variance of the band-
 309 pass filtered 700 hPa meridional wind over 2-6 days is also visible, indicating African easterly wave
 310 activity (Reed et al., 1977). Other studies also point out that rainfall fluctuations in equatorial
 311 Africa are associated with Kelvin waves (Jackson et al., 2019). The residual term could influence the
 312 estimation of dynamic and thermodynamic distributions in the water budget, and its high values in
 313 the Sahel region would be associated with a non-linear interaction between wind and. ~~Analysis of~~
 314 ~~the components of the water balance over the western part of the Congo Basin (6°S-5°N, 6°-20°E)~~
 315 ~~for October 2019 (Fig. 6) shows that the increase in rainfall was dominated by vertical advection of~~
 316 ~~moisture induced by changes in humidity, vertical velocity~~ $\langle -\omega' \partial_p \bar{q} \rangle$ (-1.4 mm/day). However,
 317 ~~the contributions of the other processes, including the residual term, are low.~~

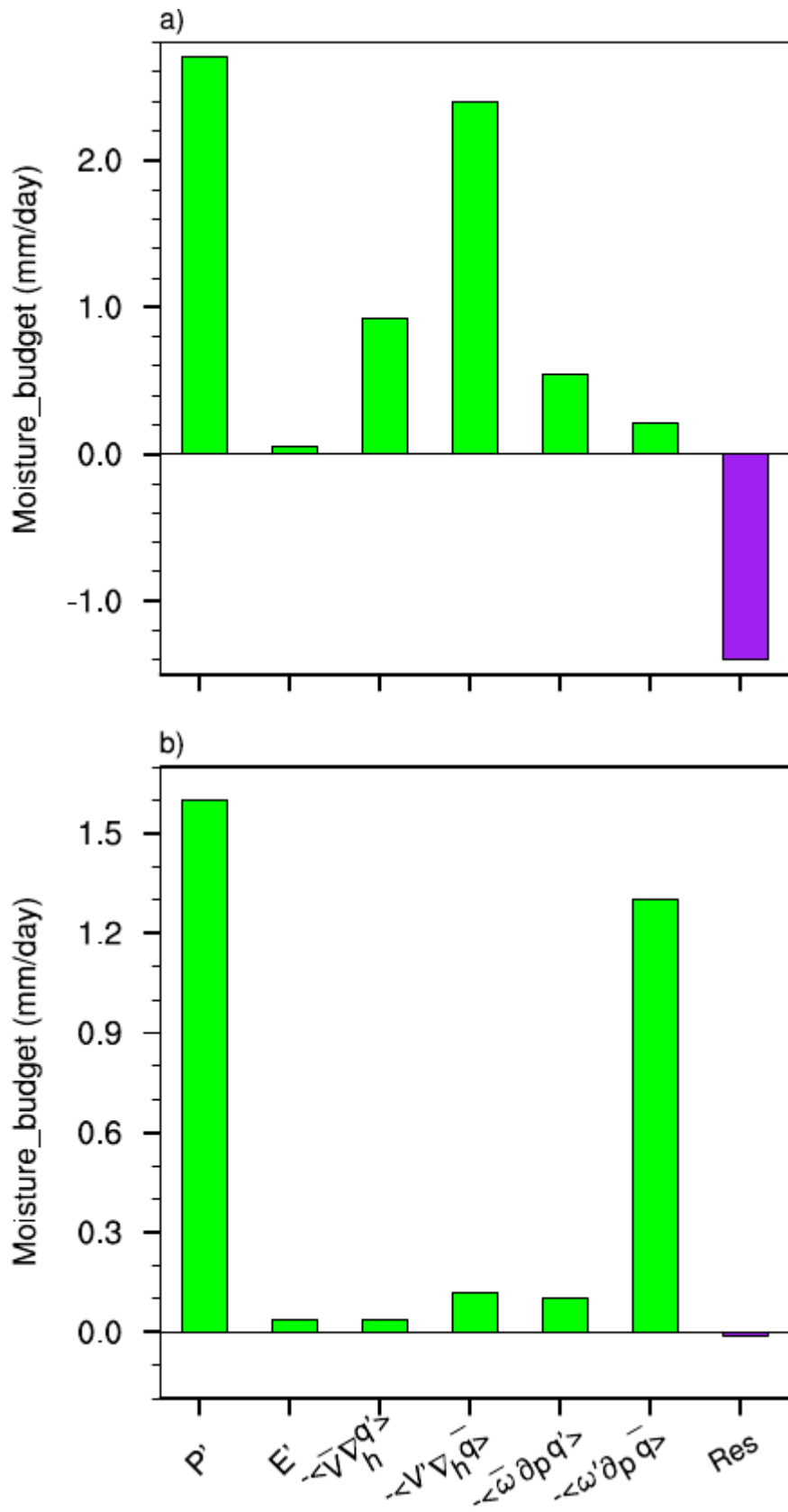
318 Analysis of the components of the water balance over the western part of the Congo Basin
 319 (6°S-5°N, 6°-20°E) for October 2019 (Fig. 5b) shows that the increase in rainfall was dominated by
 320 vertical advection of moisture induced by changes in vertical velocity $\langle -\omega' \partial_p \bar{q} \rangle$ (1.4 mm/day).
 321 However, the contributions of the other processes, including the residual term, are low.

322



323

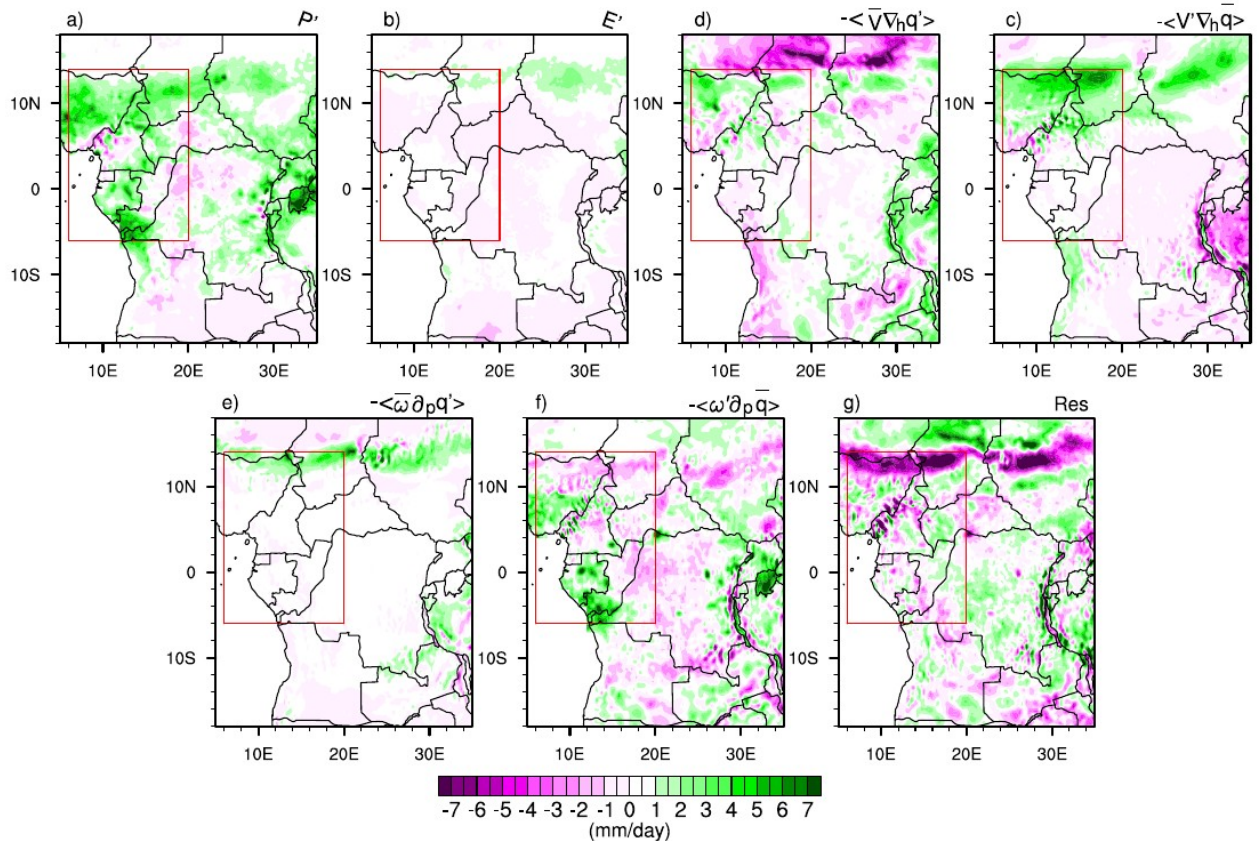
324 **Fig. 5** Monthly mean anomalies in moisture budget for October 2019, averaged over the Northern-
 325 part of West Central Africa (6°N-14°N, 6°-20°E).-



326

327 **Fig. 56:** Monthly mean anomalies in moisture budget for October 2019, averaged in a) over the
 328 Northern part of West Central Africa (6°N-14°N, 6°-20°E) and b) over the Southern part of West
 329 Central Africa (6°S-5°N, 6°-20°E).

330 At the pixel scale, positive precipitation anomalies over eastern Nigeria, southern Chad and
 331 northern Cameroon (Fig. 6a7a) were mainly dominated by horizontal moisture advection induced
 332 by the horizontal wind anomaly (Fig. 6d7d). Over Gabon, south of Congo Brazzaville, positive
 333 precipitation anomalies were dominated by vertical moisture advection induced by vertical
 334 anomalous motion (Fig. 6f7f). Horizontal moisture advection induced by the specific humidity
 335 anomaly (Fig. 6c7c), although not the key factor associated with precipitation patterns, shows a
 336 small positive contribution over the northern part of the domain.



337
 338 **Fig. 67.** Spatial distributions of each term of the water budget equation during October 2019 over West
 339 Equatorial Africa (Red box). (a) Precipitation anomalies, (b) evaporation anomaly, (c) horizontal
 340 advection of anomalous moisture by climatological wind, (d) horizontal advection of climatological
 341 moisture by anomalous wind, (e) vertical advection of anomalous moisture by climatological vertical
 342 velocity, (f) vertical advection of climatological moisture by anomalous vertical velocity and (g) the
 343 residual term.

344
 345 The contribution of evaporation (Fig. 6b7b) and horizontal advection of moisture induced by the
 346 specific humidity anomaly (Fig. 6c7c) remains weak over the entire domain, although some positive

347 values can be seen around 14°N. This result is similar to that provided by MERRA2 (Figure S2).
348 Thermodynamic effects reflect the change in the thermal state of the atmosphere associated with the
349 October 2019 rainfall extremes over West Central Africa. ~~It should be noted that changes in the~~
350 ~~thermal state of the atmosphere may allow us to speculate on the potential role of global warming in~~
351 ~~rainfall variations in 2019, even without considering potential impacts on atmospheric dynamics.~~
352 However, changes in the thermodynamic effect, although not the key factor responsible for the
353 October 2019 events, contributed up to 35% of the total effect (the sum of dynamic and
354 thermodynamic contributions) on the northern part and 15% on the southern part of the domain.
355 This could be since the increase in diabatic heating contributes to the change in the thermal state
356 of the atmosphere, i.e. the increase in thermodynamic effects (changes in humidity). In fact,
357 Nicholson et al. (2022) reported that the increase in SST in the tropical Atlantic strengthened the
358 advection of moist air from the Atlantic towards the region, with an increase in the moisture flux
359 from the west to southwest.

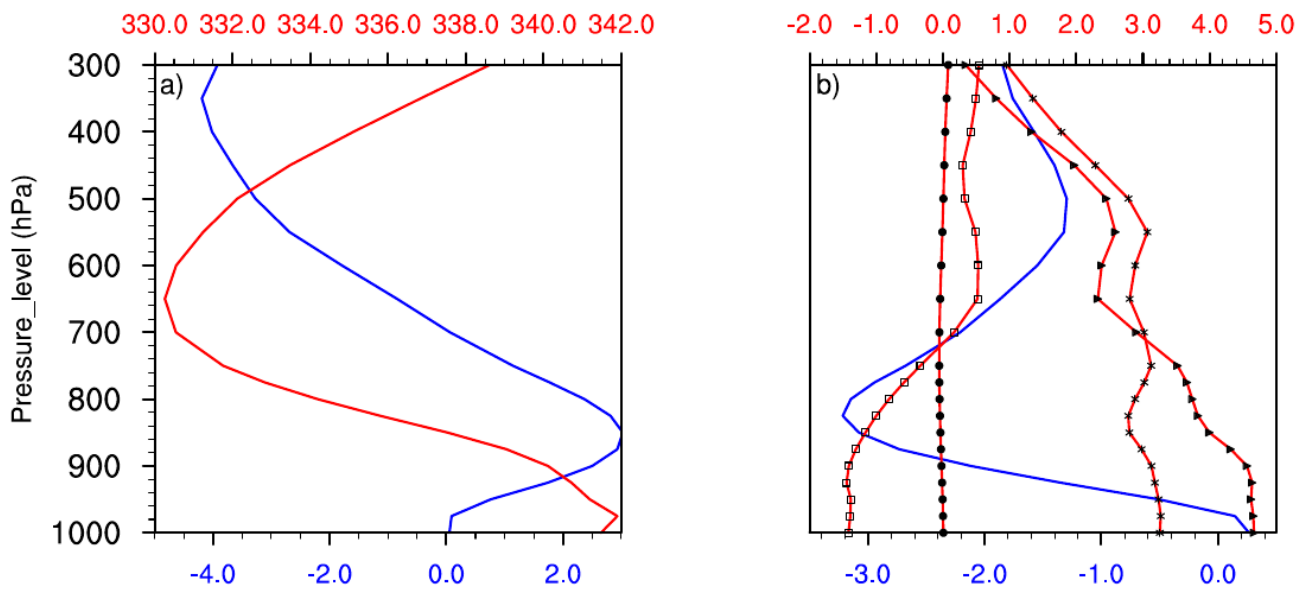
360

361 5 MSE budget analysis

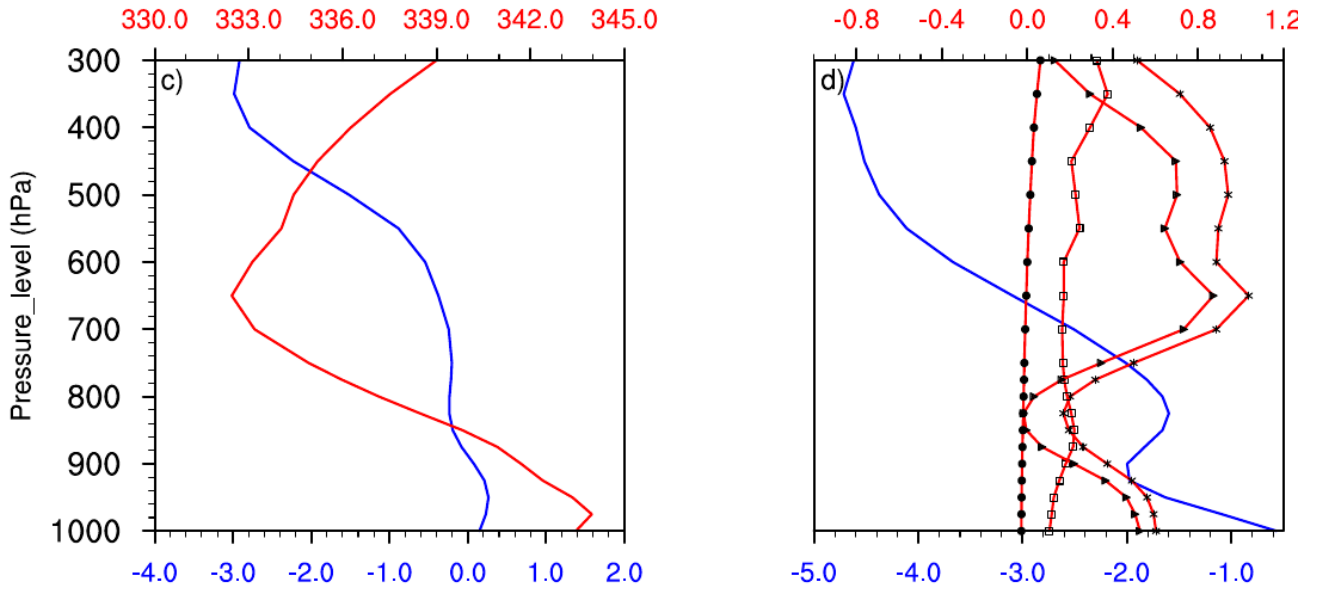
362 The previous results clearly showed that the vertical advection of moisture induced by the
363 vertical velocity anomaly was identified as the second dynamic parameter (after the horizontal
364 advection of moisture induced by the anomalous horizontal movement) contributing to the
365 increase in precipitation in October 2019. Diagnosis of the MSE budget, which takes account of the
366 thermal state of the atmosphere and the effect of atmospheric circulation, is used to analyse the
367 atmospheric perturbation related to moisture transport. The MSE largely influences the structure of
368 vertical motion. In addition, diagnosis of the MSE balance emphasises the relative contributions of
369 temperature, specific humidity and atmospheric circulation associated with the vertical motion
370 anomaly.

371 The vertical profiles of the vertical velocity anomaly ω' and the MSE climatology \bar{m}
372 averaged over the north of the domain are shown in Figure [7a8a](#). The vertical velocity anomaly ω'
373 shows positive values at the surface and negative values in the middle and upper troposphere. The
374 alternation of positive and negative values in the tropospheric column probably reduces the
375 contribution of the vertical advection of moisture induced by the anomalous vertical motion. The
376 MSE climatology \bar{m} exhibits a bottom-heavy ~~bore~~ structure with a minimum around 650 hPa.
377 Such a structure generally indicates that $\langle \partial_p \bar{m} \rangle < 0$ (Chen and Bordoni, 2014; Liu et al. 2021; Wen

378 et al. 2022). As a result, positive (negative) values of $\langle \omega' \partial_p \bar{m} \rangle$ depends on the vertical structure of
 379 the omega anomalies. The vertical velocity climatology $\bar{\omega}$ (Fig. 7b8b) is negative over the entire
 380 troposphere, characterising an upward movement. The MSE anomaly m' decreased slightly near
 381 the surface then increased from 800 hPa to 550 hPa, with a minimum value around 550 hPa.
 382 However, this includes three terms, namely, gz' which is weak in the entire tropospheric column,
 383 the enthalpy anomaly $c_p T'$, which tends to increase, and $l_v q'$, tends to behave similarly to m'
 384 between 650 hPa and 300 hPa. To the south of the domain (Fig. 7c8e), the vertical velocity anomaly
 385 shows negative



386



387

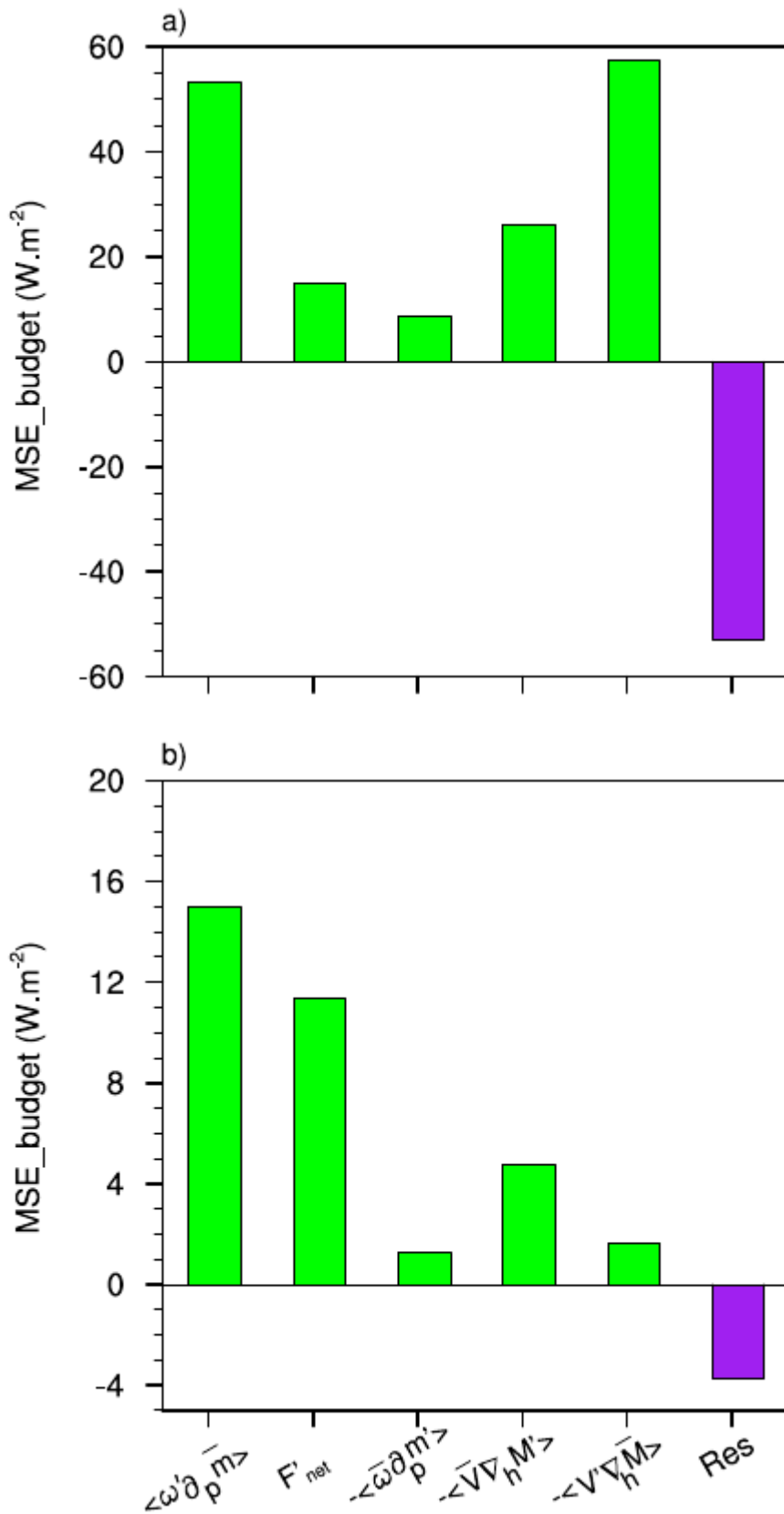
388 **Fig. 78.** Vertical profile of a) vertical velocity anomaly ω' (blue line: $10^{-2} Pa.s^{-1}$) and MSE
 389 climatology \bar{m} (red line: $10^3 J.Kq^{-1}$), and b) vertical velocity climatology $\bar{\omega}$ (blue line:
 390 $10^{-2} Pa.s^{-1}$), MSE anomaly m' (line with stars: $10^3 J.Kq^{-1}$), enthalpy anomaly $c_p T'$ (line with
 391 squares: $10^3 J.Kq^{-1}$), latent energy anomaly $l_v q'$ (line with triangles: $10^3 J.Kq^{-1}$) and
 392 geopotential anomaly Ψ' (line with dark circle: $10^3 J.Kq^{-1}$) averaged over the Northern part of
 393 West Central Africa (6°N-14°N, 6°-20°E) and c), d) the same parameters averaged over the
 394 Southern part of West Central Africa (6°S-5°N, 6°-20°E) during October 2019.

395

396 values from 900 hPa up to the upper troposphere, accelerating the anomalous vertical movement.
 397 The structure of the MSE climatology is similar to that observed to the north, with a maximum of
 398 around 650 hPa. The vertical profiles (Fig. 7d8d) of the MSE anomaly and the latent energy
 399 anomaly show similar structures throughout the tropospheric column, with maximum values at 650
 400 hPa.

401 Based on the contributions of the different terms in equation 9 to the MSE over the northern
 402 part of West Central Africa (Fig. 8a9), the advection of wet enthalpy induced by the horizontal
 403 wind anomalies $-\langle \mathbf{V}' \cdot \nabla M \rangle$ is the main term contributing most to the vertical advection of the
 404 MSE induced by the vertical velocity anomaly $\langle \omega' \partial_p \bar{m} \rangle$. This is confirmed by the high correlation
 405 ($r = 0.6$) between the two terms compared to the other terms.

406 We also note the contribution of the thermodynamic terms, although the horizontal advection of the
407 MSE induced by the wet enthalpy variation $-\langle \nabla \cdot \nabla M' \rangle$ dominates ($r = 0.3$) compared to the
408 vertical advection of the MSE induced by the MSE variation $-\langle \omega \partial_p m' \rangle$ ($r = -0.2$). A weak
409 contribution from the net flow of energy is noticeable ($r = 0.18$). This could be due to the fact that
410 the energy in the radiative and turbulent heat fluxes penetrating the atmosphere over West Central
411 Africa has suffered a loss linked to the increase in cloud cover, which has a strong influence on
412 short-wave radiation. Such a reduction in energy in the air column has an impact on upward motion.
413 This result is in line with that of Wen et al. (2022) and Sheng et al. (2023), who pointed to a
414 reduction in the net energy in the air column during the exceptional rainy season in the summer of
415 2020 in the Yangtze River valley and the anomalous increase in precipitation over southern China
416 in 2022. However, as with the moisture balance, the residual term is also considerable.



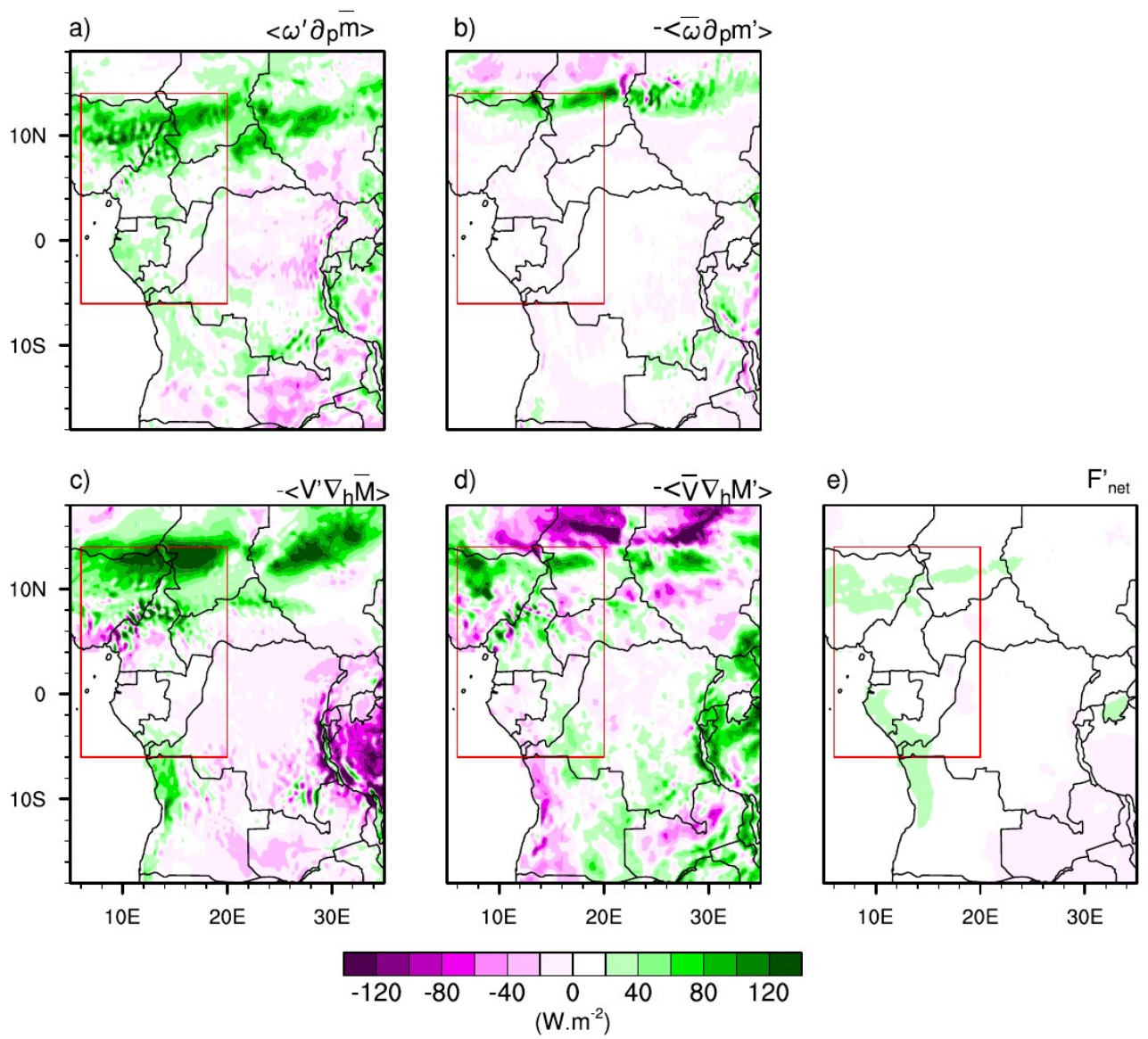
417
 418 **Fig. 8.** Different terms of the Moist Static Energy (MSE) budget averaged in a) over the Northern
 419 part of West Central Africa (6°N-14°N, 6°-20°E) and b) over the Southern part of West Central
 420 Africa (6°S-5°N, 6°-20°E).

421

422 To the south of the domain(Fig. 8b), the increase in the net energy balance was responsible for
423 strengthening the vertical advection of the MSE induced by the vertical velocity anomaly ($r = 0.51$).

424 In addition, the increase in vertical movement was reinforced by an increase in the horizontal
425 advection of the MSE induced by the variation in wet enthalpy $-\langle \nabla \cdot \nabla M' \rangle$. This is in agreement
426 with the results of Kenfack et al. (2024) who highlighted the importance of horizontal advections in
427 the MSE and moisture flux as well as their implications for vertical motion over the Congo Basin.
428 The contributions in vertical advection induced by changes in the MSE and horizontal advection
429 induced by changes in the horizontal wind are small. Moreover, similarly to the moisture flux
430 advected in the western part of the Congo Basin, the residual term was less important in the MSE
431 budget compared to the northern part.

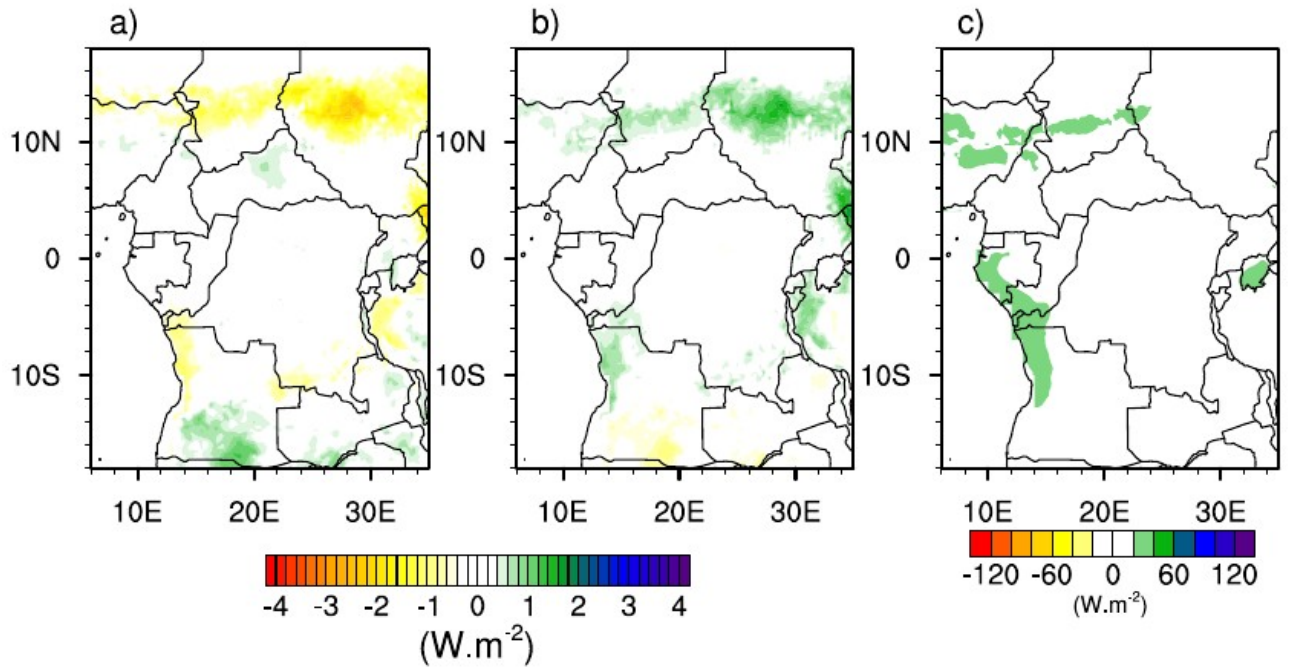
432 On a regional scale, the vertical advection of the MSE induced by the vertical motion anomaly
433 $\langle \omega' \partial_p \bar{m} \rangle$ (Fig. 9a) is mainly dominated by the dynamic term $-\langle \mathbf{V}' \cdot \nabla M \rangle$ (Fig. 9c), which brings



436 **Fig. 9.** Spatial distributions of each term of the Moist Static Energy (MSE) balance equation during
 437 October 2019 over West Equatorial Africa (Red box). (a) vertical advection of climatological MSE
 438 by anomalous vertical velocity, (b) vertical advection of anomalous MSE by climatological vertical
 439 velocity, (c) horizontal advection of anomalous moist enthalpy by climatological wind, (e) horizontal
 440 advection of climatological moist enthalpy by anomalous wind, and (f) net energy flux (at the surface
 441 and top of the atmosphere) in the atmospheric column.

442 There is a high concentration of positive values in both dynamic terms, up to $120 \text{ W}\cdot\text{m}^{-2}$ in the
 443 north of West Central Africa. In addition, the two thermodynamic terms $-\langle \omega \partial_p m' \rangle$ (Fig. 9b) and
 444 $-\langle \nabla \cdot \nabla M' \rangle$ (Fig. 9d), although weak, also contributed to reinforcing the vertical advection of
 445 MSE induced by the vertical motion anomaly. It should be remembered that the term $-\langle \omega \partial_p m' \rangle$
 446 remains very weak over the region as a whole, except the northern part where a slight layer of
 447 positive values can be observed. Terms $-\langle \mathbf{V}' \cdot \nabla \bar{M} \rangle$, $-\langle \nabla \cdot \nabla M' \rangle$ and $-\langle \omega \partial_p m' \rangle$ in the MSE
 448 have a similar spatial distribution to terms $\langle -\mathbf{V}' \cdot \nabla \bar{q} \rangle$, $\langle -\nabla \cdot \nabla q' \rangle$ and $\langle -\bar{\omega} \partial_p q' \rangle$ in the
 449 moisture, which is in agreement with the findings of Kenfack et al. (2024). The difference between
 450 the net energy balance for 2019 and the climatology (Fig. 9e) shows low positive values in the north
 451 and south of the region respectively. Such an increase (mainly to the south of the area) is associated
 452 with a strengthening in the vertical structure of the MSE anomaly through ascending currents and,
 453 consequently, an increase in precipitation. A further analysis of the net energy balance (Fig. 10)
 454 shows that during October 2019, the latent heat flux (Fig. 10a) decreased mainly over the Sahel and
 455 to the south of the domain. Sensible heat, on the other hand, increased slightly, with values of
 456 around $1.5 \text{ W}\cdot\text{m}^{-2}$. Analysis of the radiative flux anomalies shows strong positive values over the
 457 Sahel and the southern part of the domain (up to $50 \text{ W}\cdot\text{m}^{-2}$), showing that this is the main factor
 458 responsible for the increase in the energy balance during the exceptional event of October 2019.

459



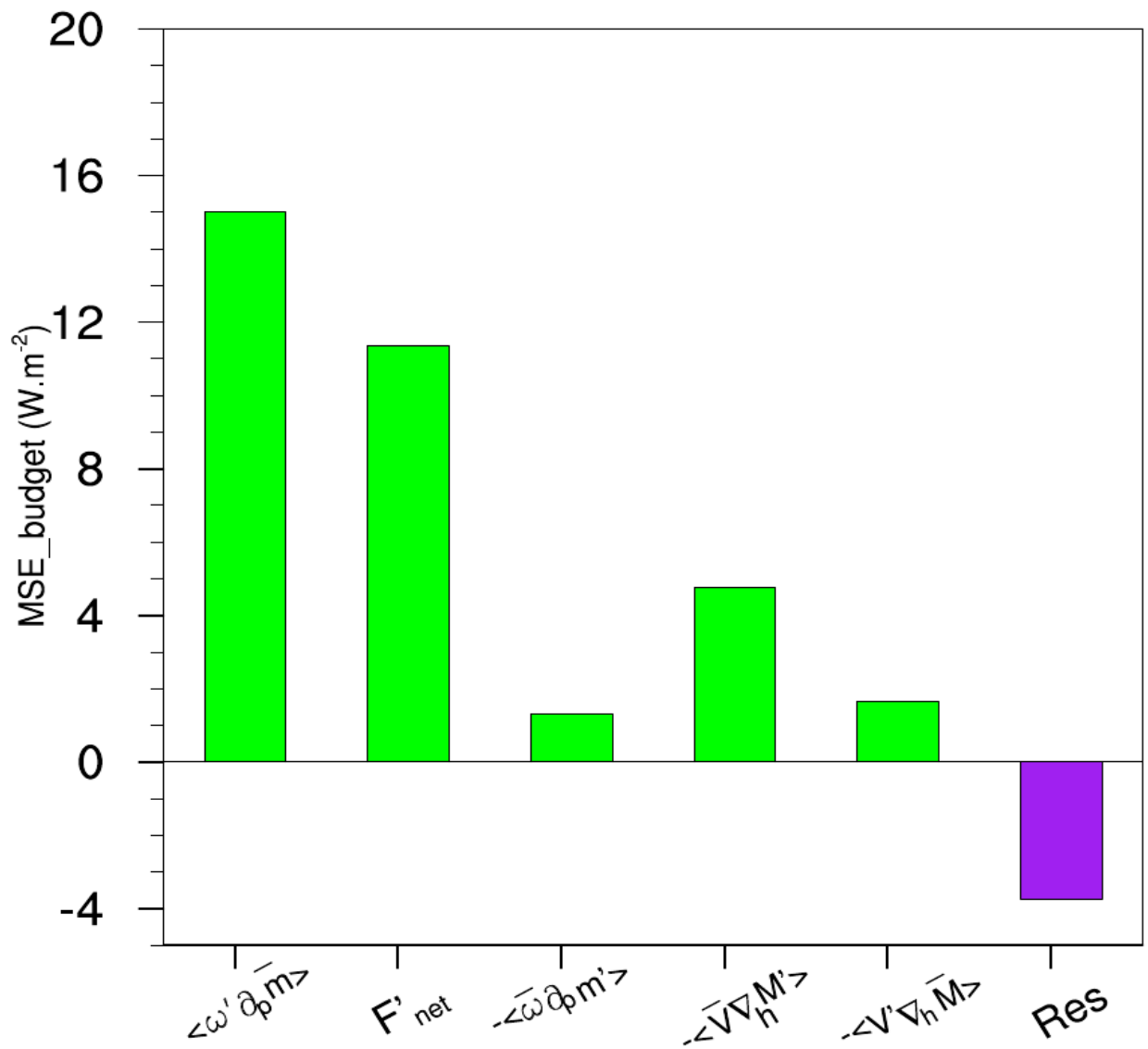
460

461 Fig. 10. Spatial distribution of a) latent heat, b) sensible heat and c) radiative flux anomalies in
 462 October 2019 over western equatorial Africa.

463 Although the dynamic contribution is the most important, the thermodynamic contribution cannot
 464 be neglected. This would mean that the interaction between atmospheric dynamic and
 465 thermodynamic variables would induce significant indirect effects on October 2019 precipitation
 466 anomalies over West Central Africa.

467 Fig. 9. Different terms of the Moist Static Energy (MSE) budget averaged over the Northern part of
 468 West Central Africa (6°N-14°N, 6°-20°E).

469 ~~We also note the contribution of the thermodynamic terms, although the horizontal advection of the~~
 470 ~~MSE induced by the wet enthalpy variation $-\langle \nabla \cdot \nabla M' \rangle$ dominates ($r=0.3$) compared to the~~
 471 ~~vertical advection of the MSE induced by the MSE variation $-\langle \omega \partial_p m' \rangle$ ($r=-0.2$). A weak~~
 472 ~~contribution from the net flow of energy is noticeable ($r=0.18$). This could be due to the fact that~~
 473 ~~the energy in the radiative and turbulent heat fluxes penetrating the atmosphere over West Central~~
 474 ~~Africa has suffered a loss linked to the increase in cloud cover, which has a strong influence on~~
 475 ~~short-wave radiation. Such a reduction in energy in the air column has an impact on upward motion.~~



476

477 **Fig. 10.** Different terms of the Moist Static Energy (MSE) budget averaged over the Southern part
 478 of West Central Africa (6°S-5°N, 6°-20°E).

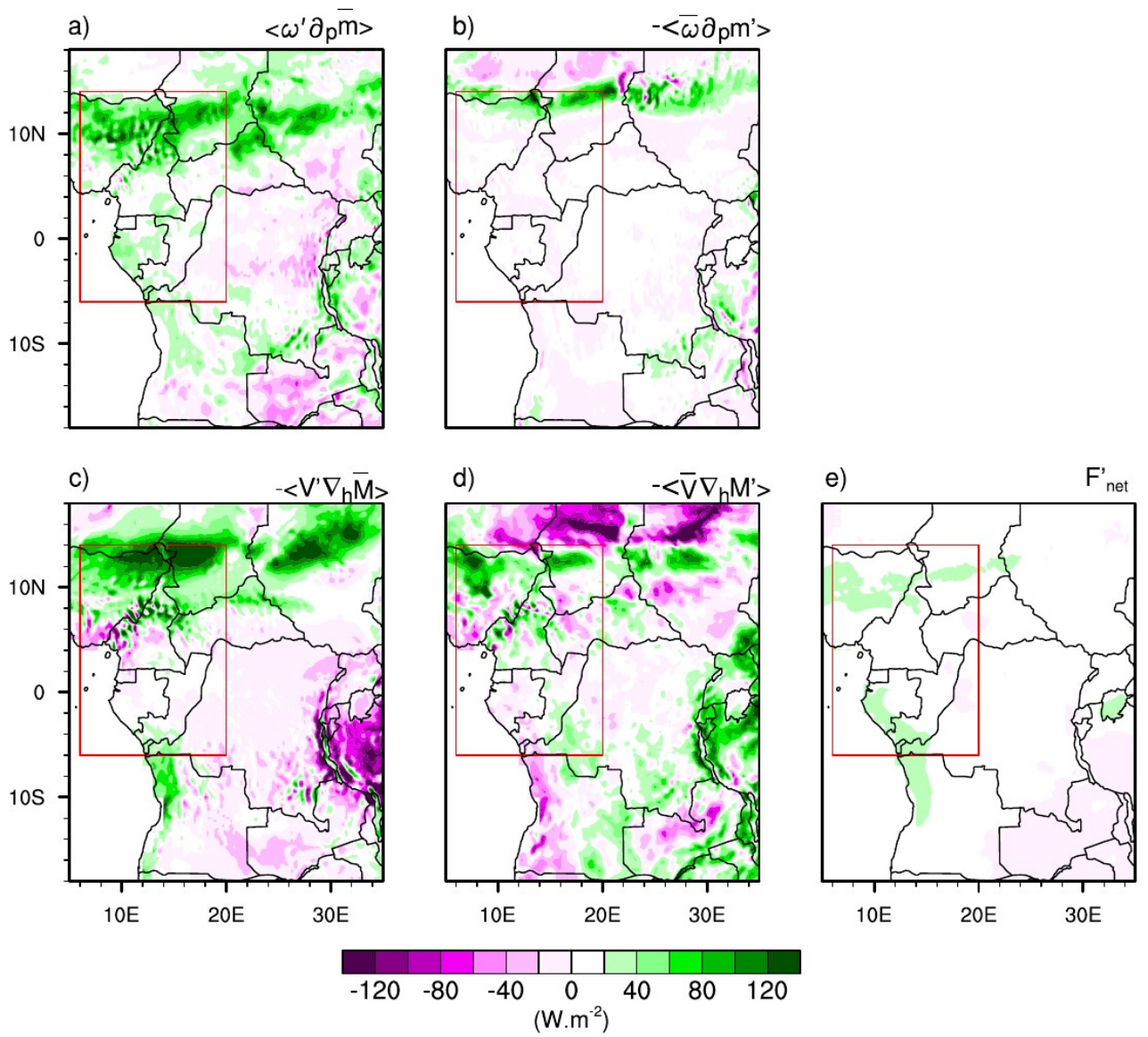
479

480 This result is in line with that of Wen et al. (2022) and Sheng et al. (2023), who pointed to a
 481 reduction in the net energy in the air column during the exceptional rainy season in the summer of
 482 2020 in the Yangtze River valley and the anomalous increase in precipitation over southern China
 483 in 2022. However, as with the moisture balance, the residual term is also considerable:

484 —To the south of the domain(Fig. 10), the increase in the net energy balance was responsible for
 485 strengthening the vertical advection of the MSE induced by the vertical velocity anomaly ($r = 0.51$).
 486 In addition, the increase in vertical movement was reinforced by an increase in the horizontal
 487 advection of the MSE induced by the variation in wet enthalpy $-\langle \bar{V} \cdot \nabla_h M' \rangle$. This is in agreement

488 | with the results of Kenfack et al. (2024) who highlighted the importance of horizontal advections in
489 | the MSE and moisture flux as well as their implications for vertical motion over the Congo Basin.
490 | The contributions in vertical advection induced by changes in the MSE and horizontal advection
491 | induced by changes in the horizontal wind are small. Moreover, similarly to the moisture flux
492 | advected in the western part of the Congo Basin, the residual term was less important in the MSE
493 | budget compared to the northern part.

494 | — On a regional scale, the vertical advection of the MSE induced by the vertical motion anomaly
495 | $\langle \omega' \partial_p \bar{m} \rangle$ (Fig. 11a) is mainly dominated by the dynamic term $-\langle \mathbf{V}' \cdot \nabla \bar{M} \rangle$ (Fig. 11c), which



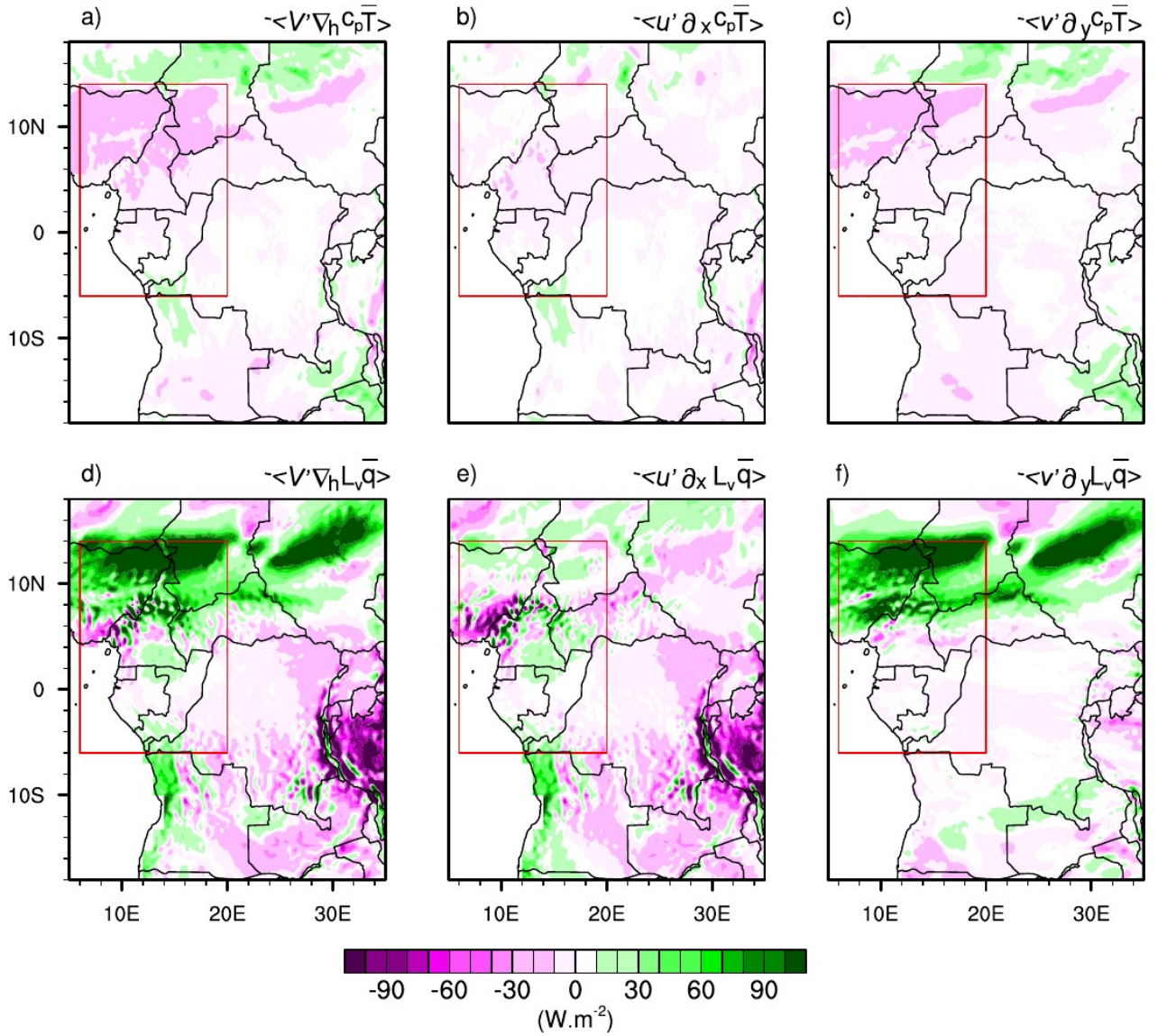
498 **Fig. 11.** Spatial distributions of each term of the Moist Static Energy (MSE) balance equation during
 499 October 2019 over West Equatorial Africa (Red box). (a) vertical advection of climatological MSE
 500 by anomalous vertical velocity, (b) vertical advection of anomalous MSE by climatological vertical
 501 velocity, (c) horizontal advection of anomalous moist enthalpy by climatological wind, (e) horizontal
 502 advection of climatological moist enthalpy by anomalous wind, and (f) net energy flux (at the surface
 503 and top of the atmosphere) in the atmospheric column.

504

505 There is a high concentration of positive values in both dynamic terms, up to $120 \text{ W} \cdot \text{m}^{-2}$ in the
 506 north of West Central Africa. In addition, the two thermodynamic terms $-\langle \omega \partial_p m' \rangle$ (Fig. 11b)
 507 and $-\langle \nabla \cdot \nabla M' \rangle$ (Fig. 11d), although weak, also contributed to reinforcing the vertical advection
 508 of MSE induced by the vertical motion anomaly. It should be remembered that the term
 509 $-\langle \omega \partial_p m' \rangle$ remains very weak over the region as a whole, except the northern part where a slight
 510 layer of positive values can be observed. Terms $-\langle \mathbf{V}' \cdot \nabla M \rangle$, $-\langle \nabla \cdot \nabla M' \rangle$ and $-\langle \omega \partial_p m' \rangle$ in
 511 the MSE have a similar spatial distribution to terms $\langle -\mathbf{V}' \cdot \nabla \bar{q} \rangle$, $\langle -\nabla \cdot \nabla q' \rangle$ and $\langle -\omega \partial_p q' \rangle$
 512 in the moisture, which is in agreement with the findings of Kenfack et al. (2024). The difference
 513 between the net energy balance for 2019 and the climatology (Fig. 11e) shows low positive values
 514 in the north and south of the region respectively. Such an increase (mainly to the south of the area)
 515 is associated with a strengthening in the vertical structure of the MSE anomaly through ascending
 516 currents and, consequently, an increase in precipitation. Although the dynamic contribution is the
 517 most important, the thermodynamic contribution cannot be neglected. This would mean that the
 518 interaction between atmospheric dynamic and thermodynamic variables would induce significant
 519 indirect effects on October 2019 precipitation anomalies over West Central Africa.

520 5.1 Dynamic effect

521 The aforementioned results clearly show that enthalpy advection induced by the horizontal wind
 522 anomaly is crucial in understanding the processes at the origin of October 2019 extreme
 523 precipitation over northern part of West Central Africa. It should be remembered that, as we
 524 mentioned in the diagnostic section of the MSE balance, the wet enthalpy $M = c_p T + L_v q$ results
 525 from the sum of the dry enthalpy and the latent heat. Thus, the horizontal advection of wet enthalpy
 526 induced by the wind anomaly can be separated into two terms: dry enthalpy $-\langle \mathbf{V}' \cdot \nabla_h c_p T \rangle$ (Fig.
 527 [11a+2a](#)) and latent heat $-\langle \mathbf{V}' \cdot \nabla_h l_v \bar{q} \rangle$ (Fig. [11d+2d](#)).



528

529 | **Fig. 11f2.** Horizontal advection of (a–c) climatological dry enthalpy and (d–f) latent energy by
 530 anomalous wind, designated as a dynamic effect during October 2019 over West Central Africa
 531 (Red box). (a, d) Total advection, (b, e) zonal component, and (c, f) meridional component.

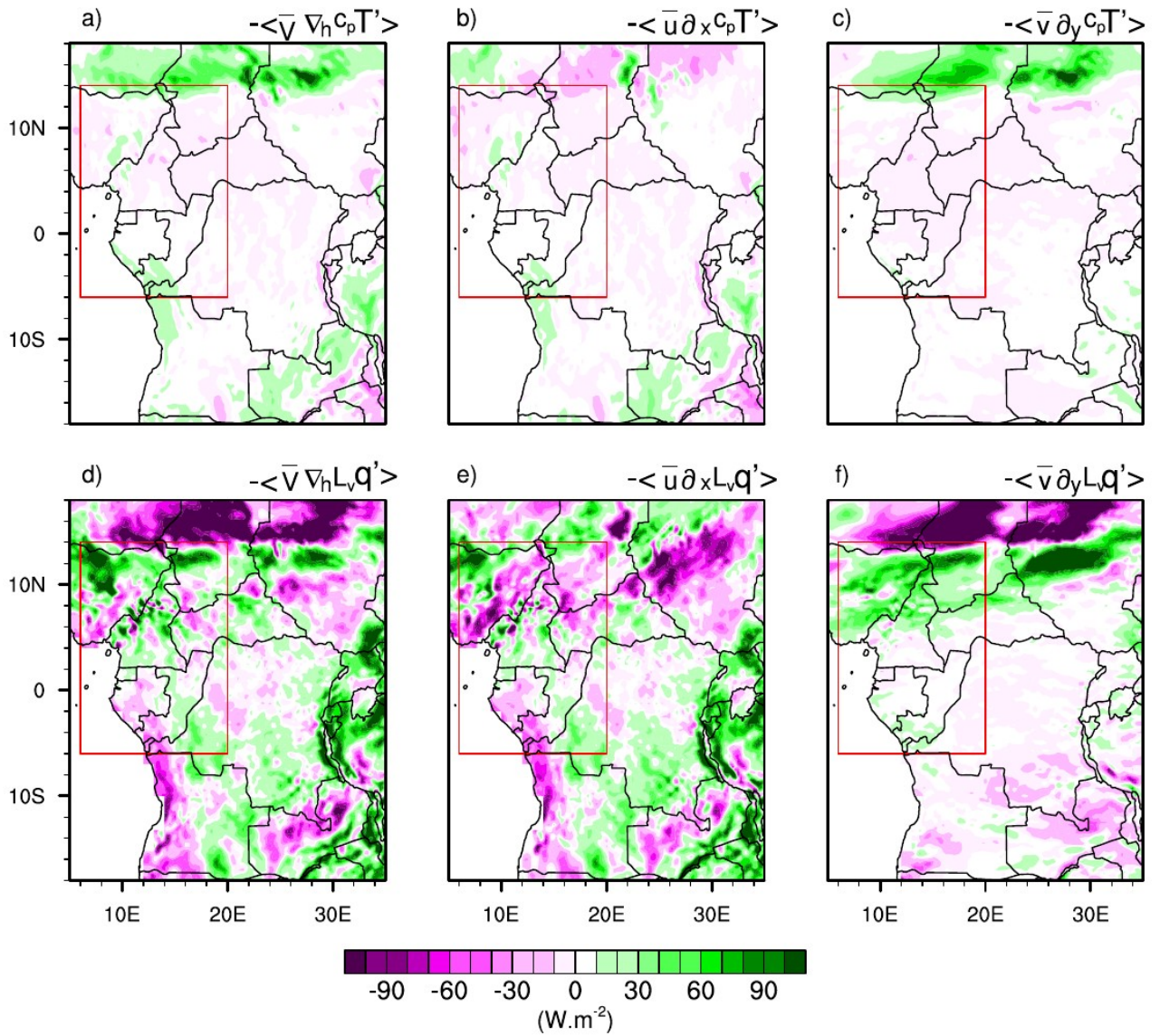
532

533 Given the influence of the wind anomaly components on the displacement of dry enthalpy and
 534 latent heat, a further decomposition of the $-\langle \mathbf{v}' \cdot \nabla_h c_p T \rangle$ and $-\langle \mathbf{v}' \cdot \nabla_h l_v \bar{q} \rangle$ terms along the
 535 zonal (Figs. 11b+2b,e) and meridional (Figs. 11c+2c,f) directions appear necessary. Figure 11a+2a
 536 shows that the advection of dry enthalpy induced by the horizontal wind anomaly decreased over
 537 the area-averaged, with the highest values between 6°N and 14°N. The advection of dry enthalpy by
 538 the meridional wind anomaly (Fig. 11c+2c) is particularly responsible for the decrease in the

539 $-\langle \mathbf{V}' \cdot \nabla_h c_p T' \rangle$ term compared with the advection of dry enthalpy induced by the zonal wind
540 anomaly (Fig. [11b+12b](#)), which is weak. For the transport of latent heat (Fig. [11d+12d](#)), the influence
541 of the advection of $-\langle \mathbf{V}' \cdot \nabla_h l_v \bar{q}' \rangle$ term under the effect of the anomalous meridional circulation
542 is the main term responsible for the supply of moist air to the northern part of the area, while the
543 low contribution to the south is associated with a low input of moist air from the zonal wind
544 anomaly (Fig. [11f+12f](#)). Analysis of the advection of dry enthalpy and latent heat by anomalous
545 winds shows that the meridional wind anomaly had a significant impact compared with the zonal
546 wind anomaly. In addition, the advection of the dynamic term associated with latent heat
547 contributed significantly to the supply of MSE to West Central Africa compared to the advection of
548 the dynamic term associated with dry enthalpy. One of the reasons would be because in addition to
549 the warm Atlantic SSTs, there was also an anomalous meridional mean sea level pressure (MSLP)
550 gradient in the Central African Sahel between a lower MSLP over the eastern Sahara and a higher
551 pressure between 10 and 15°N. In addition, the trans-equatorial meridional wind fluctuated with the
552 activity of the African easterly waves over the Gulf of Guinea (Nicholson et al. 2022).

553 5.2 Thermodynamic effect

554 The results of the previous section highlighted the importance of dynamics, particularly in a
555 meridional direction, on extreme precipitation in October 2019. However, we previously also
556 observed that the thermodynamic contribution should not be neglected. Similar to the previous
557 section, the thermodynamic term $-\langle \mathbf{V}' \cdot \nabla M' \rangle$ (i.e. the advection of the wet enthalpy anomaly
558 associated with wind climatology) can also be separated into two terms, namely: Dry enthalpy
559 $-\langle \mathbf{V}' \cdot \nabla_h c_p T' \rangle$ (Fig. [12a+13a](#)) and latent heat $-\langle \mathbf{V}' \cdot \nabla_h l_v \bar{q}' \rangle$ (Fig. [12d+13d](#)).



560

561 | **Fig. 1213.** As in Fig. 1142, but for the thermodynamic effect (horizontal advection of anomalous dry
 562 enthalpy and latent energy by climatological wind) during October 2019 over West Central Africa
 563 (Red box).

564

565 To better assess the contribution of each term, we split the horizontal wind into zonal and
 566 meridional directions. The advection of the dry enthalpy anomaly by the horizontal zonal and
 567 meridional wind components is shown in Figures 12b and 12c, 13b and 13e, respectively. It can also
 568 be seen that the dry enthalpy anomaly is very small over the whole area. On the other hand, the
 569 advection of the latent heat anomaly by the horizontal wind climatology is more pronounced.
 570 Variations in latent heat are strong in the meridional direction, while the zonal direction shows a
 571 reduction in abnormal latent heat. This could be due to the strong meridional wind associated with

572 the increase in SST in the tropical Atlantic, which results in strong advection of water vapor into
573 West Central Africa, leading to precipitation. The reduction in advection of the latent heat anomaly
574 on the Atlantic coast is amplified by the zonal wind climatology. However, the advection of the wet
575 enthalpy induced by the horizontal wind anomaly (dynamic effect) is stronger than the advection of
576 the wet enthalpy anomaly by the wind climatology. As a result, we note in particular the changes in
577 the meridional wind for the dynamic effect and the latent heat associated with the warming of the
578 equatorial Atlantic for the thermodynamic effect.

579 **6 Summary and concluding remarks**

580 West Central Africa was hit by unprecedented exceptional rainfall in October 2019. A few
581 studies have investigated the meteorological causes associated with these extreme rainfall events
582 (Wainwright et al, 2020; Nicholson et al. 2022). This study followed these perspectives and focused
583 on evaluating the dynamic and thermodynamic processes that controlled the extreme events of
584 2019. We proceeded by decomposing the water balance and MSE equation, separating the
585 associated dynamic and thermodynamic effects. Changes in atmospheric circulation are behind
586 dynamic processes, while changes in water vapor are behind thermodynamic processes. This
587 approach provides a better understanding of the mechanisms behind rainfall anomalies. ~~The
588 thermodynamic effect, in particular, can be used to speculate on the influence of global warming on
589 heavy rainfall in October 2019, notably on the increase in the temperature of the troposphere and its
590 water vapor content.~~ The main findings can be summarised as follows:

- 591 1. The main feature of October 2019 in the northern part of the area was a strong southerly
592 circulation compared with the typical climatology for 1988-2017. In addition, a more
593 pronounced rate of humidity associated with significant diabatic heating over West Central
594 Africa up to 15°N was recorded.
- 595 2. The diagnosis of the water balance reveals that the exceptional rainfall in October 2019 was
596 mainly dominated by dynamic effects. However, moisture advection induced by horizontal
597 wind anomalies is the dominant process of precipitation anomalies over the northern part of
598 the zone, while vertical moisture advection induced by vertical velocity anomalies is the
599 dominant process of precipitation extremes in the south, mainly over Gabon and southern
600 Congo Brazzaville. Changes in the thermodynamic effect, although not the key factor
601 responsible for the events of October 2019, contribute up to 35% of the total effect (the sum
602 of the dynamic and thermodynamic contributions) on the northern part and 15% on the
603 southern part of the domain. The contribution of evaporation remains weak in both areas

604 combined, which allows us to conclude that evaporation was not responsible for the heavy
605 rainfall of October 2019 in West Central Africa.

606 3. The MSE vertical advection anomaly is dominated over the northern part of the area by the
607 dynamic term (i.e. the advection of the wet enthalpy induced by the horizontal wind
608 anomalies) compared to the thermodynamic terms (i.e. the horizontal advection of the MSE
609 induced by the variation of the wet enthalpy and the vertical advection of the MSE induced
610 by the variation of the MSE). In the southern part, the increase in the net energy balance
611 compared with the climatology is the dominant process that has contributed most to the
612 change in the structure of the vertical anomaly of the MSE. The prevailing net balance is
613 controlled by the anomalies in radiative flux compared with the anomalies in latent and
614 sensible heat flux. An extended analysis shows that these variations in the MSE over the
615 north of West Central Africa were governed by its meridional component, in particular the
616 variations in the meridional wind in the dynamic effect and the meridional variations in
617 latent heat in the thermodynamic effect. It should be pointed out that in both cases, the
618 contribution of dry enthalpy helped to reduce the dynamic term and was small in the
619 thermodynamic term.

620 The results of this study show that moisture advection induced by horizontal wind anomalies and
621 vertical moisture advection induced by vertical velocity anomaly were crucial mechanisms in the
622 anomalous October 2019 exceptional rainfall increase over West Central Africa. In addition,
623 changes in the MSE budget, mainly through the meridional circulation (dynamic effect), and latent
624 heat (thermodynamic effect) also played an important role in the northern part of the area, while the
625 increase in the energy balance contributed considerably to the change in the MSE balance in the
626 southern part of the area. However, there was little contribution from dry enthalpy. These results are
627 consistent with those of Nicholson et al (2022) who showed that the increase in equatorial Atlantic
628 SSTs associated with the late retreat of the West African monsoon played an important role in
629 precipitation anomalies in the Sahel. Changes in SSTs along the east coast of the equatorial Atlantic
630 display a similar pattern to the Atlantic Niño as described by Lutz et al. (2013). Furthermore,
631 Vallès-Casanova et al (2020) also highlighted the fact that 2019 was characterised by a particularly
632 intense Atlantic Niño, which lasted until October, placing the dynamic and thermodynamic
633 processes in the context of the large-scale circulation. The importance of the dynamic contribution
634 during extreme precipitation events has been reported in other regions, notably over southern China
635 (Wen et al. 2022; Sheng et al. 2023). This calls for comprehensive evaluations of both dynamic and

636 thermodynamic contributions, and their possible feedback, to assess the potential impact of climate
637 change on extreme precipitation events in this region.

638

639 **Acknowledgements.** The authors thank all the observational and reanalysis data providers used in
640 this study, and the research of the International Joint Laboratory “Dynamics of Terrestrial
641 Ecosystems in Central Africa: A Context of Global Changes” (IJL DYCOCA/LMI DYCOFAC).

642

643 **Competing Interests.** The authors declare that they have no conflict of interest.

644

645 **Authors' contributions**

646 **Kevin Kenfack:** Conceptualization; data analysis; formal analysis; investigation; methodology;
647 writing - original draft; review and editing.

648 **Francesco Marra:** Supervision; conceptualization; investigation; writing – review and editing.

649 **Zéphirin Yepdo Djomou:** Investigation; writing; review and editing; supervision; validation.

650 **Lucie A. Djotang Tchotchou:** Validation; supervision; methodology; writing – review and editing.

651 **Alain T. Tamoffo:** Conceptualization; investigation; methodology; project administration; resources;
652 supervision; validation; review and editing.

653 **Derbetini A. Vondou:** Project administration; supervision; resources; validation; methodology;
654 writing – review and editing.

655

656 **Funding.** Not applicable

657

658 | _____

659 | **Code availability**

660 | Figures shown in this study are plotted using the NCAR Command Language (NCL,
661 | <https://doi.org/10.5065/D6WD3XH5>, The NCAR Command Language, 2017). Codes can be
662 | obtained from the corresponding author.

663 |

664 | **Data Availability Statement**

665

666 The **ERA5** reanalysis is produced within the Copernicus Climate Change Service (C3S) by the
667 ECMWF and is accessible via the link [https://cds.climate.copernicus.eu/cdsapp#!/dataset/reanalysis-
era5-pressure-levels-monthly-means?tab1/4form](https://cds.climate.copernicus.eu/cdsapp#!/dataset/reanalysis-
668 era5-pressure-levels-monthly-means?tab1/4form).

669

670 **References**

671

673 Andrews, P. C., Cook, K. H., and Vizy, E. K.: Mesoscale convective systems in the Congo Basin:
674 Seasonality, regionality, and diurnal cycles, *Clim. Dynam.*, 62, 609–630,
675 <https://doi.org/10.1007/s00382-023-06903-7>, 2023.

676

677 Kenya – over 100 dead, 18,000 displaced after recent floods and landslides – floodlist:
678 <http://floodlist.com/africa/kenya-floods-november-2019>, last access: 2 April 2024.

679

680 Aretouyap, Z., Kemgang, F. E. G., Domra, J. K., Bisso, D., and Njandjock, P. N.: Understanding the
681 occurrences of fault and landslide in the region of West-Cameroon using remote sensing and GIS
682 techniques, *Nat. Hazards*, 109, 1589–1602, <https://doi.org/10.1007/s11069-021-04890-8>, 2021.

683

684 Bell, J. P., Tompkins, A. M., Bouka-Biona, C., and Sanda, I. S.: A process-based investigation into
685 the impact of the Congo basin deforestation on surface climate, *J. Geophys. Res-Atmos.*, 120, 5721–
686 5739, <https://doi.org/10.1002/2014jd022586>, 2015.

687

688 Black, E.: The relationship between Indian Ocean sea–surface temperature and East African rainfall,
689 *Philos. T. R. Soc. A*, 363, 43–47, <https://doi.org/10.1098/rsta.2004.1474>, 2005.

690

691 Chadwick, R., Good, P., and Willett, K.: A simple moisture advection model of specific humidity
692 change over land in response to SST warming, *J. Climate*, 29, 7613–7632,
693 <https://doi.org/10.1175/jcli-d-16-0241.1>, 2016.

694

695 Chen, J. and Bordoni, S.: Orographic effects of the Tibetan plateau on the east Asian summer
696 monsoon: An energetic perspective, *J. Climate*, 27, 3052–3072, [https://doi.org/10.1175/jcli-d-13-
00479.1](https://doi.org/10.1175/jcli-d-13-
697 00479.1), 2014.

698

699 Cook, K. H. and Vizy, E. K.: Hydrodynamics of regional and seasonal variations in Congo Basin

700 precipitation, *Clim. Dynam.*, 59, 1775–1797, <https://doi.org/10.1007/s00382-021-06066-3>, 2021.
701

702 Cook, K. H., Liu, Y., and Vizzy, E. K.: Congo Basin drying associated with poleward shifts of the
703 African thermal lows, *Clim. Dynam.*, 54, 863–883, <https://doi.org/10.1007/s00382-019-05033-3>,
704 2019.
705

706 Dyer, E. L. E., Jones, D. B. A., Nusbaumer, J., Li, H., Collins, O., Vettoretti, G., and Noone, D.:
707 Congo Basin precipitation: Assessing seasonality, regional interactions, and sources of moisture, *J.*
708 *Geophys. Res-Atmos.*, 122, 6882–6898, <https://doi.org/10.1002/2016jd026240>, 2017.
709

710 Fontaine, B., Roucou, P., and Trzaska, S.: Atmospheric water cycle and moisture fluxes in the West
711 African monsoon: Mean annual cycles and relationship using NCEP/NCAR reanalysis, *Geophys.*
712 *Res. Lett.*, 30, <https://doi.org/10.1029/2002gl015834>, 2003.
713

714 Fotso-Nguemo, T. C., Chamani, R., Yepdo, Z. D., Sonkoué, D., Matsaguim, C. N., Vondou, D. A.,
715 and Tanessong, R. S.: Projected trends of extreme rainfall events from CMIP5 models over Central
716 Africa, *Atmos. Sci. Lett.*, 19, <https://doi.org/10.1002/asl.803>, 2018.
717

718 Fotso-Nguemo, T. C., Diallo, I., Diakhaté, M., Vondou, D. A., Mbaye, M. L., Haensler, A., Gaye, A.
719 T., and Tchawoua, C.: Projected changes in the seasonal cycle of extreme rainfall events from
720 CORDEX simulations over Central Africa, *Climatic. Change*, 155, 339–357,
721 <https://doi.org/10.1007/s10584-019-02492-9>, 2019.
722

723 Funk, C., Peterson, P., Landsfeld, M., Pedreros, D., Verdin, J., Shukla, S., Husak, G., Rowland, J.,
724 Harrison, L., Hoell, A., and Michaelsen, J.: The climate hazards infrared precipitation with stations—
725 a new environmental record for monitoring extremes, *Scientific Data*, 2,
726 <https://doi.org/10.1038/sdata.2015.66>, 2015.
727

728 Garcin, Y., Deschamps, P., Ménot, G., de Saulieu, G., Schefuß, E., Sebag, D., Dupont, L. M.,
729 Oslisly, R., Brademann, B., Mbusnum, K. G., Onana, J.-M., Ako, A. A., Epp, L. S., Tjallingii, R.,
730 Strecker, M. R., Brauer, A., and Sachse, D.: Early anthropogenic impact on Western Central African
731 rainforests 2,600 y ago, *P. Natl. A. Sci. India. A*, 115, 3261–3266,
732 <https://doi.org/10.1073/pnas.1715336115>, 2018.
733

734 [Gelaro, R., McCarty, W., Suárez, M. J., Todling, R., Molod, A., Takacs, L., Randles, C. A.,](#)
735 [Darmenov, A., Bosilovich, M. G., Reichle, R., Wargan, K., Coy, L., Cullather, R., Draper, C.,](#)
736 [Akella, S., Buchard, V., Conaty, A., da Silva, A. M., Gu, W., Kim, G.-K., Koster, R., Lucchesi, R.,](#)
737 [Merkova, D., Nielsen, J. E., Partyka, G., Pawson, S., Putman, W., Rienecker, M., Schubert, S. D.,](#)
738 [Sienkiewicz, M., and Zhao, B.: The Modern-Era Retrospective Analysis for Research and](#)
739 [Applications, Version 2 \(MERRA-2\), *J. Climate*, 30, 5419–5454, \[https://doi.org/10.1175/jcli-d-16-\]\(https://doi.org/10.1175/jcli-d-16-0758.1\)](#)
740 [0758.1, 2017.](#)

741
742

743 Gou, Y., Balling, J., De Sy, V., Herold, M., De Keersmaecker, W., Slagter, B., Mullissa, A., Shang,
744 X., and Reiche, J.: Intra-annual relationship between precipitation and forest disturbance in the
745 African rainforest, *Environ. Res. Lett.*, 17, 044044, <https://doi.org/10.1088/1748-9326/ac5ca0>, 2022.
746

747 Harris, I., Osborn, T. J., Jones, P., and Lister, D.: Version 4 of the CRU TS monthly high-resolution
748 gridded multivariate climate dataset, *Scientific Data*, 7, <https://doi.org/10.1038/s41597-020-0453-3>,
749 2020.
750

751 He, Y., Tian, W., Huang, J., Wang, G., Ren, Y., Yan, H., Yu, H., Guan, X., and Hu, H.: The
752 mechanism of increasing summer water vapor over the Tibetan plateau, *J. Geophys. Res-Atmos.*,
753 126, <https://doi.org/10.1029/2020jd034166>, 2021.
754

755 Hersbach, H., Bell, B., Berrisford, P., Hirahara, S., Horányi, A., Muñoz-Sabater, J., Nicolas, J.,
756 Peubey, C., Radu, R., Schepers, D., Simmons, A., Soci, C., Abdalla, S., Abellan, X., Balsamo, G.,
757 Bechtold, P., Biavati, G., Bidlot, J., Bonavita, M., De Chiara, G., Dahlgren, P., Dee, D., Diamantakis,
758 M., Dragani, R., Flemming, J., Forbes, R., Fuentes, M., Geer, A., Haimberger, L., Healy, S., Hogan,
759 R. J., Hólm, E., Janisková, M., Keeley, S., Laloyaux, P., Lopez, P., Lupu, C., Radnoti, G., de Rosnay,
760 P., Rozum, I., Vamborg, F., Villaume, S., and Thépaut, J.: The ERA5 global reanalysis, *Q. J. Roy.*
761 *Meteor. Soc.*, 146, 1999–2049, <https://doi.org/10.1002/qj.3803>, 2020.
762

763 Hua, W., Zhou, L., Nicholson, S. E., Chen, H., and Qin, M.: Assessing reanalysis data for
764 understanding rainfall climatology and variability over Central Equatorial Africa, *Clim. Dynam.*, 53,
765 651–669, <https://doi.org/10.1007/s00382-018-04604-0>, 2019.
766

767 Huffman, G. J., Adler, R. F., Bolvin, D. T., and Gu, G.: Improving the global precipitation record:

768 GPCP Version 2.1, *Geophys. Res. Lett.*, 36, <https://doi.org/10.1029/2009gl040000>, 2009.
769

770 Jackson, B., Nicholson, S. E., and Klotter, D.: Mesoscale convective systems over Western
771 Equatorial Africa and their relationship to large-scale circulation, *Mon. Weather. Rev.*, 137, 1272–
772 1294, <https://doi.org/10.1175/2008mwr2525.1>, 2009.
773

774 Jiang, J., Zhou, T., Chen, X., and Zhang, L.: Future changes in precipitation over Central Asia based
775 on CMIP6 projections, *Environ. Res. Lett.*, 15, 054009, <https://doi.org/10.1088/1748-9326/ab7d03>,
776 2020.
777

778 Johannsen, Ermida, Martins, Trigo, Nogueira, and Dutra: Cold bias of ERA5 summertime daily
779 maximum land surface temperature over Iberian Peninsula, *Remote. Sens.-Basel*, 11, 2570,
780 <https://doi.org/10.3390/rs11212570>, 2019.
781

782 Kamae, Y., Mei, W., and Xie, S.-P.: Climatological relationship between warm season atmospheric
783 rivers and heavy rainfall over East Asia, *J. Meteorol. Soc. Jpn., Ser. II*, 95, 411–431,
784 <https://doi.org/10.2151/jmsj.2017-027>, 2017.
785

786 Kenfack, K., Tamoffo, A. T., Djiotang Tchotchou, L. A., and Vondou, D. A.: Assessment of
787 uncertainties in reanalysis datasets in reproducing thermodynamic mechanisms in the moisture
788 budget's provision in the Congo Basin, *Theor. Appl. Climatol.*, 154, 613–626,
789 <https://doi.org/10.1007/s00704-023-04576-0>, 2023.
790

791 Kenfack, K., Tamoffo, A. T., Tchotchou, L. A. D., Marra, F., Kaissassou, S., Nana, H. N., and
792 Vondou, D. A.: Processes behind the decrease in Congo Basin precipitation during the rainy seasons
793 inferred from ERA-5 reanalysis, *Int. J. Climatol.*, <https://doi.org/10.1002/joc.8410>, 2024.
794

795 Kuete, G., Pokam Mba, W., and Washington, R.: African Easterly Jet South: Control, maintenance
796 mechanisms and link with Southern subtropical waves, *Clim. Dynam.*, 54, 1539–1552,
797 <https://doi.org/10.1007/s00382-019-05072-w>, 2019.
798

799 Li, P., Zhou, T., and Chen, X.: Water vapor transport for spring persistent rains over southeastern
800 China based on five reanalysis datasets, *Clim. Dynam.*, 51, 4243–4257,
801 <https://doi.org/10.1007/s00382-017-3680-3>, 2017.

802

803 Liu, S., Wen, N., and Li, L.: Dynamic and thermodynamic contributions to Northern China dryness
804 in El Niño developing summer, *Int. J. Climatol.*, 41, 2878–2890, <https://doi.org/10.1002/joc.6995>,
805 2021.

806

807 Longandjo, G.-N. T. and Rouault, M.: Revisiting the seasonal cycle of rainfall over Central Africa, *J.*
808 *Climate*, 37, 1015–1032, <https://doi.org/10.1175/jcli-d-23-0281.1>, 2024.

809

810 Lutz, K., Rathmann, J., and Jacobeit, J.: Classification of warm and cold water events in the eastern
811 tropical Atlantic Ocean, *Atmos. Sci. Lett.*, 14, 102–106, <https://doi.org/10.1002/asl2.424>, 2013.

812

813 Mariotti, L., Diallo, I., Coppola, E., and Giorgi, F.: Seasonal and intraseasonal changes of African
814 monsoon climates in 21st century CORDEX projections, *Climatic. Change*, 125, 53–65,
815 <https://doi.org/10.1007/s10584-014-1097-0>, 2014.

816

817 Marra, F., Levizzani, V., and Cattani, E.: Changes in extreme daily precipitation over Africa: Insights
818 from a non-asymptotic statistical approach, *J. Hydrol. X*, 16, 100130,
819 <https://doi.org/10.1016/j.hydroa.2022.100130>, 2022.

820

821 Moon, S. and Ha, K.-J.: Future changes in monsoon duration and precipitation using CMIP6, *NPJ*
822 *Clim. Atmos. S.*, 3, <https://doi.org/10.1038/s41612-020-00151-w>, 2020.

823

824 Moudi Pascal, I., Kammalac Jores, T., Talib, J., Appolinaire, V. D., Hirons, L., Christian, N., Tene
825 Romeo-Ledoux, D., Fogang Michael, T., Marceline, M., Tanessong Roméo, S., Dione, C.,
826 Thompson, E., Salih, A. A. M., and Ngaryamgaye, S.: Strengthening weather forecast and
827 dissemination capabilities in Central Africa: Case assessment of intense flooding in January 2020,
828 *Climate Services*, 32, 100411, <https://doi.org/10.1016/j.cliser.2023.100411>, 2023.

829

830 Nana, H. N., Tanessong, R. S., Tchotchou, L. A. D., Tamoffo, A. T., Moihamette, F., and Vondou,
831 D. A.: Influence of strong South Atlantic Ocean Dipole on the Central African rainfall's system,
832 *Clim. Dynam.*, 62, 1–16, <https://doi.org/10.1007/s00382-023-06892-7>, 2023.

833

834 Neelin, J. D.: Moist dynamics of tropical convection zones in monsoons, teleconnections, and global

835 warming, in: *The Global Circulation of the Atmosphere*, Princeton University Press, 267–301, 2021.
836

837 Ngandam Mfondoum, A. H., Wokwenmendiam Nguet, P., Mefire Mfondoum, J. V., Tchindjang, M.,
838 Hakdaoui, S., Cooper, R., Gbetkom, P. G., Penaye, J., Bekoa, A., and Moudioh, C.: Adapting sudden
839 landslide identification product (SLIP) and detecting real-time increased precipitation (DRIP)
840 algorithms to map rainfall-triggered landslides in Western Cameroon highlands (Central-Africa),
841 *Geoenvironmental Disasters*, 8, <https://doi.org/10.1186/s40677-021-00189-9>, 2021.
842

843 Nicholson, S. E., Fink, A. H., Funk, C., Klotter, D. A., and Satheesh, A. R.: Meteorological causes of
844 the catastrophic rains of October/November 2019 in equatorial Africa, *Global. Planet. Change*, 208,
845 103687, <https://doi.org/10.1016/j.gloplacha.2021.103687>, 2022.
846

847 Oueslati, B., Yiou, P., and Jézéquel, A.: Revisiting the dynamic and thermodynamic processes
848 driving the record-breaking January 2014 precipitation in the southern UK, *Sci. Rep-Uk.*, 9,
849 <https://doi.org/10.1038/s41598-019-39306-y>, 2019.
850

851 Pokam, W. M., Djiotang, L. A. T., and Mkankam, F. K.: Atmospheric water vapor transport and
852 recycling in Equatorial Central Africa through NCEP/NCAR reanalysis data, *Clim. Dynam.*, 38,
853 1715–1729, <https://doi.org/10.1007/s00382-011-1242-7>, 2011.
854

855 Pokam, W. M., Bain, C. L., Chadwick, R. S., Graham, R., Sonwa, D. J., and Kamga, F. M. (2014):
856 Identification of processes driving low-level westerlies in West Equatorial Africa, *J. Climate*, 27,
857 4245–4262, <https://doi.org/10.1175/jcli-d-13-00490.1>, 2014.
858

859 Seager, R., Naik, N., and Vecchi, G. A.: Thermodynamic and dynamic mechanisms for large-scale
860 changes in the hydrological cycle in response to global warming*, *J. Climate*, 23, 4651–4668,
861 <https://doi.org/10.1175/2010jcli3655.1>, 2010.
862

863 Sheng, B., Wang, H., Li, H., Wu, K., and Li, Q.: Thermodynamic and dynamic effects of anomalous
864 dragon boat water over South China in 2022, *Weather and Climate Extremes*, 40, 100560,
865 <https://doi.org/10.1016/j.wace.2023.100560>, 2023.
866

867 Sonkoué, D., Monkam, D., Fotso-Nguemo, T. C., Yepdo, Z. D., and Vondou, D. A.: Evaluation and
868 projected changes in daily rainfall characteristics over Central Africa based on a multi-model

869 ensemble mean of CMIP5 simulations, *Theor. Appl. Climatol.*, 137, 2167–2186,
870 <https://doi.org/10.1007/s00704-018-2729-5>, 2018.

871

872 Taguela, T. N., Pokam, W. M., and Washington, R.: Rainfall in uncoupled and coupled versions of
873 the Met Office Unified Model over Central Africa: Investigation of processes during the September–
874 November rainy season, *Int. J. Climatol.*, 42, 6311–6331, <https://doi.org/10.1002/joc.7591>, 2022.

875

876 Tamoffo, A. T., Vondou, D. A., Pokam, W. M., Haensler, A., Yepdo, Z. D., Fotso-Nguemo, T. C., ...
877 ~~Fehotchou, L. A. D., and Nouayou, R. (2019). Daily characteristics of Central African rainfall in the~~
878 ~~REMO model. *Theoretical and Applied Climatology*, 137(3–4), *Theor. Appl. Climatol.*, 137, 2351–~~
879 ~~2368, <https://doi.org/10.1007/s00704-018-2745-5>, 2019.~~

880

881 [Tamoffo, A. T., Weber, T., Akinsanola, A. A., & Vondou, D. A. \(2023\). Projected changes in](#)
882 [extreme rainfall and temperature events and possible implications for Cameroon’s socio-economic](#)
883 [sectors. *Meteorological Applications*, 30\(2\). <https://doi.org/10.1002/met.2119>](#)

884

885 [Tamoffo, A. T., Dosio, A., Weber, T., & Vondou, D. A. \(2023b\). Dynamic and thermodynamic](#)
886 [contributions to late 21st century projected rainfall change in the congo basin: Impact of a regional](#)
887 [climate model’s formulation. *Atmosphere*, 14\(12\), 1808. <https://doi.org/10.3390/atmos14121808>](#)

888

889 [Tamoffo, A. T., Weber, T., Cabos, W., Sein, D. V., Dosio, A., Rechid, D., ... Jacob, D. \(2024\).](#)
890 [Mechanisms of added value of a coupled global ocean-regional atmosphere climate model over](#)
891 [Central Equatorial Africa. *Journal of Geophysical Research: Atmospheres*, 129\(3\).](#)
892 <https://doi.org/10.1029/2023jd039385>

893 ~~Tamoffo, A. T., Weber, T., Akinsanola, A. A., and Vondou, D. A.: Projected changes in extreme-~~
894 ~~rainfall and temperature events and possible implications for Cameroon’s socio-economic sectors,~~
895 ~~*Meteorol. Appl.*, 30, <https://doi.org/10.1002/met.2119>, 2023.~~

896

897 Vallès-Casanova, I., Lee, S., Foltz, G. R., and Pelegrí, J. L.: On the Spatiotemporal Diversity of
898 Atlantic Niño and Associated Rainfall Variability Over West Africa and South America, *Geophys.*
899 *Res. Lett.*, 47, <https://doi.org/10.1029/2020gl087108>, 2020.

900

901 Wainwright, C. M., Finney, D. L., Kilavi, M., Black, E., and Marsham, J. H.: Extreme rainfall in East

902 Africa, October 2019–January 2020 and context under future climate change, *Weather*, 76, 26–31,
903 <https://doi.org/10.1002/wea.3824>, 2020.

904

905 Wang, L. and Li, T.: Effect of vertical moist static energy advection on MJO eastward propagation:
906 Sensitivity to analysis domain, *Clim. Dynam.*, 54, 2029–2039, [https://doi.org/10.1007/s00382-019-](https://doi.org/10.1007/s00382-019-05101-8)
907 05101-8, 2020a.

908

909 Wang, T. and Li, T.: Diagnosing the column-integrated moist static energy budget associated with
910 the northward-propagating boreal summer intraseasonal oscillation, *Clim. Dynam.*, 54, 4711–4732,
911 <https://doi.org/10.1007/s00382-020-05249-8>, 2020b.

912

913 Wantim, M. N., Ughe, W. G., Kwah, D. C., Bah, T. C., Quinette, N., and Ayonghe, S. N.: Forensic
914 investigation of the Gouache landslide disaster, Western Region, Cameroon, *Journal of the*
915 *Cameroon Academy of Sciences*, 19, 223–240, <https://doi.org/10.4314/jcas.v19i3.3>, 2023.

916

917 Washington, R., James, R., Pearce, H., Pokam, W. M., and Moufouma-Okia, W.: Congo Basin
918 rainfall climatology: Can we believe the climate models?, *Philos. T. R. Soc. B.*, 368, 20120296,
919 <https://doi.org/10.1098/rstb.2012.0296>, 2013.

920

921 Wen, N., Liu, S., and Li, L. Z. X.: Diagnosing the dynamic and thermodynamic effects for the
922 exceptional 2020 summer rainy season in the Yangtze River Valley, *J. Meteorol. Res-Prc.*, 36, 26–
923 36, <https://doi.org/10.1007/s13351-022-1126-2>, 2022.

924

925 Yanai, M. and Tomita, T.: Seasonal and interannual variability of atmospheric heat sources and
926 moisture sinks as determined from NCEP–NCAR reanalysis, *J. Climate*, 11, 463–482,
927 [https://doi.org/10.1175/1520-0442\(1998\)011<0463:saivoa>2.0.co;2](https://doi.org/10.1175/1520-0442(1998)011<0463:saivoa>2.0.co;2), 1998.

928

929 Zhao, D., Zhang, L., and Zhou, T.: Detectable anthropogenic forcing on the long-term changes of
930 summer precipitation over the Tibetan Plateau, *Clim. Dynam.*, 59, 1939–1952,
931 <https://doi.org/10.1007/s00382-022-06189-1>, 2022.

932

933 Zhou, L., Tian, Y., Myneni, R. B., Ciais, P., Saatchi, S., Liu, Y. Y., Piao, S., Chen, H., Vermote, E.
934 F., Song, C., and Hwang, T.: Widespread decline of Congo rainforest greenness in the past decade,
935 *Nature*, 509, 86–90, <https://doi.org/10.1038/nature13265>, 2014.

936 |

937 |

938 |

939 |

940 |

941 |

942 |